# ATG8 delipidation is dispensable for plant autophagy

Sanjana Holla[1], Yong Zou[1], Igor Sabljić[1], Jonas A Ohlsson[1], Jia Xuan Leong[2-4], Florentine Ballhaus[1], Melanie Krebs[3], Karin Schumacher[3], Suayib Üstün[5], Yasin Dagdas[6], Peter V Bozhkov[1] and Elena A Minina [1,3,¶]

[1]Department of Molecular Sciences, Uppsala BioCenter, Swedish University of Agricultural Sciences and Linnean Center for Plant Biology, Uppsala, SE-750 07, Sweden
[2]Department of Algal Development and Evolution, Max Planck Institute for Biology Tübingen, Tübingen, Germany
[3]Centre for Organismal Studies (COS), Heidelberg University. Im Neuenheimer Feld 230. 69120 Heidelberg, Germany
[4]Center for Plant Molecular Biology (ZMBP), University of Tübingen, Auf der Morgenstelle 32. D-72076 Tübingen, Germany
[5]Faculty of Biology and Biotechnology, Ruhr-University Bochum, Bochum, Germany.
[6]Gregor Mendel Institute of Molecular Plant Biology, Austrian Academy of Sciences, Vienna BioCenter 1030 Vienna, Austria.
[¶]Corresponding author: Alyona Minina: alena.minina@slu.se

## Abstract

Intracellular recycling via autophagy is governed by post-translational modifications of the autophagy related (ATG) proteins. One example is ATG4-dependent delipidation of ATG8, which assumes critical but distinct roles in autophagosome formation of yeast and mammals. Here, we discovered that ATG8 delipidation is dispensable for the maturation of autophagosomes, autophagic flux and related stress tolerance in Arabidopsis. In contrast, autophagy in an evolutionary distant *Chlamydomonas* strictly required ATG4-dependent ATG8 delipidation. Additionally, we uncovered distinct participation of Arabidopsis ATG8 orthologs in autophagosome biogenesis, especially prevalent under nitrogen depletion, thereby providing new insights into potential reasons behind ATG8 gene family expansion in vascular plants.

Our findings point to evolutionary diversification of the molecular mechanism governing maturation of autophagosomes in eukaryotic lineages and highlight how this conserved pathway is tailored to diverse eukaryotic organisms.

## Introduction

Autophagy is a catabolic pathway which plays a vital role in sustaining functionality of cellular constituents and in helping organisms to overcome nutrient scarcity. Autophagy balances out the biosynthetic activity of cells and salvages nutrients by sequestering expendable or dysfunctional cytoplasmic content into double membrane-vesicles, autophagosomes, and delivering them to the lytic compartment for degradation and recycling[1]. Effective cargo sequestration relies on continuous extension of the autophagosomal membrane to create adequately sized vesicles. Subsequently, these autophagosomes must be sealed before fusing with the lytic compartment to avoid the leakage of hydrolases into the cytoplasm[2].

The process of autophagosome formation and maturation is orchestrated by the autophagy-related proteins (ATGs) conserved among all eukaryotes[1,3]. Post-translational modifications (PTMs) of the core ATGs regulate their assembly into protein complexes, which execute in a timely manner the sequential steps of autophagosome biogenesis. For example, a ubiquitin-like ATG8 protein undergoes a series of PTMs critical for elongation of the nascent autophagosomal membrane, cargo sequestration and recruitment of other core ATGs (**Fig. 1A** and **B**). The C-terminal peptide of ATG8 is removed by the dedicated protease, ATG4, producing the most abundantly present adduct, ATG8 ΔC. ATG8 ΔC has the C-terminal glycine (Gly) residue exposed for subsequent modifications[4]. Upon upregulation of autophagy, the exposed Gly of ATG8 ΔC is conjugated with the lipid phosphatidylethanolamine (PE) present on the nascent autophagosomal membranes (**Fig. 1B**)

[4,5]. The ATG8–PE conjugate is anchored in the lipid bilayer and decorates the inner and outer membranes of the forming autophagosome, playing crucial roles in cargo sequestration as well as the formation, closure, and fusion of autophagosomes[6]. At the later stages of the vesicle biogenesis, ATG4 associates with the outer membrane of the autophagosome where it cleaves the amide bond between ATG8 and PE, thereby releasing back into the cytoplasmic pool the ATG8 ΔC together with other core ATGs recruited to the membrane by ATG8 (**Fig. 1A** and **B**). This process facilitates reuse of the released proteins for formation of new autophagosomes and modifies the protein shell of the maturing autophagosome[7–9].

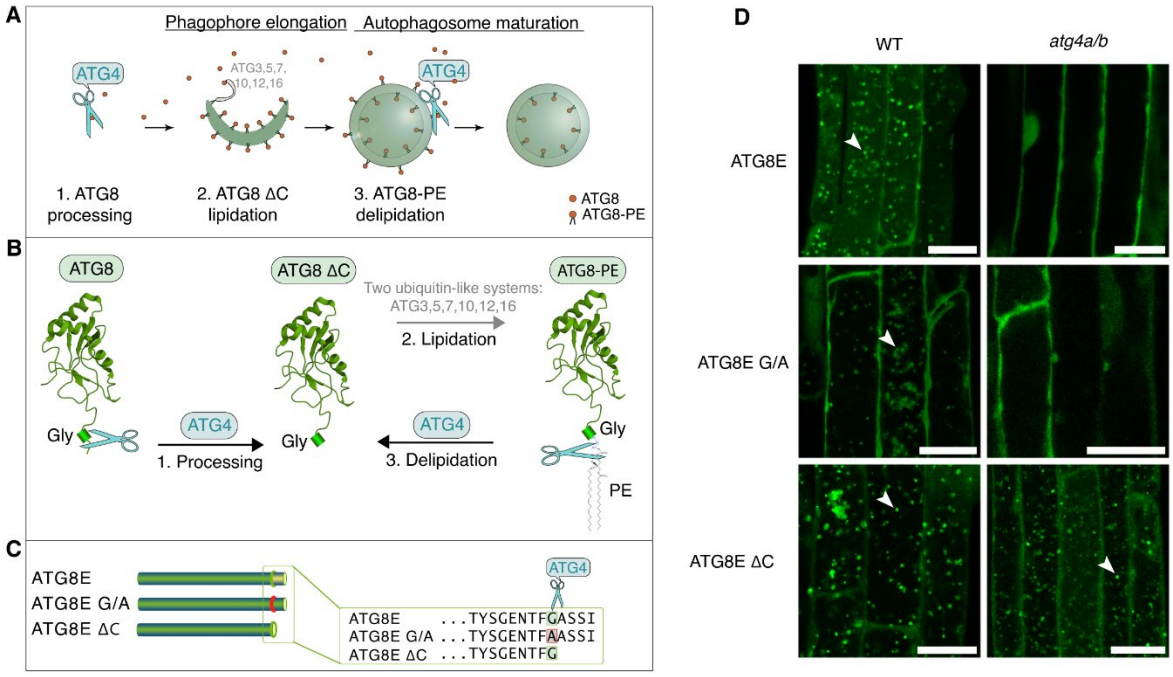


**Figure 1. Post-translational modifications of Arabidopsis ATG8 during autophagy.**

**A**. During autophagosome formation ATG8 must undergo lipidation and delipidation. Lipidation of ATG8 onto phagophore membranes is critical for phagophore elongation. To enable it, ATG8 is first proteolytically processed by ATG4. Lipidated ATG8 is then removed from the outer autophagosomal membrane during maturation of the vesicle.

**B**. ATG8 is constitutively processed by ATG4 to remove the C-terminal peptide. The obtained truncated ATG8 (ATG8 ΔC) has the C-terminal glycine residue exposed for the lipidation reaction. Lipidation of ATG8, i.e., its covalent conjugation to the phosphatidylethanolamine (PE) lipid present in the phagophore membranes (formation of ATG8–PE), is executed by two ubiquitin-like conjugation systems comprising several autophagy-related proteins, including ATG5 and ATG7. Delipidation of ATG8–PE on the outer membrane of autophagosome is performed by the ATG4 protease, which cleaves the amide bond between PE and ATG8, releasing ATG8 ΔC back into the pool of cytoplasmic ATG8 available for autophagosome biogenesis.

**C**. Diagram showing C-terminal sequences of the three artificially created variants of the Arabidopsis isoform ATG8E: ATG8E, full-length protein sequence including the C-terminal peptide masking the critical Gly; ATG8E G/A, full length protein in which the critical Gly residue was replaced with Ala; ATG8E ΔC, truncated protein lacking the C-terminal peptide that was masking the critical Gly.

**D**. Detection of three fluorescently labelled ATG8E variants (shown in **C**) in *Arabidopsis thaliana* epidermal root cells treated with AZD8055 and concanamycin A. WT, wild-type; *atg4a/b*, double knockout of ATG4A and ATG4B genes. Arrowheads indicate autophagic bodies-like puncta inside the vacuoles. Scale bars, 20 µm.

Delipidation of ATG8 has been reported to be critical for autophagy in yeast, animals, and plants[6,10,11]. Intriguingly, disruption of this conserved step stalls different stages of autophagosome biogenesis in yeast and mammalian cells. Namely, ATG4-dependent ATG8 delipidation in animal cells is critical for autophagosomal docking and fusion with

lysosomes[6,12]. However, abrogation of ATG8 delipidation in yeast impairs an earlier step of the autophagosomal membrane elongation[10,13]. This discrepancy indicates fundamental differences in maturation of yeast and animal autophagosomes and calls for further research necessary for mechanistic comprehension of the variation in the autophagosome biogenesis process among different eukaryotes.

We initiated this study with the aim to elucidate what step of autophagosome biogenesis in plants is affected by the lack of ATG8 delipidation. To our surprise, we discovered that autophagy of the vascular plant *Arabidopsis thaliana* can be carried out to its completion without ATG8 delipidation. Here we provide a thorough verification of the observed phenomenon combining cell biology, biochemistry and reverse genetics and confirm the physiological relevance of the results by plant phenotyping. Additionally, we show that delipidation remains critical for autophagy of the evolutionary distant to Arabidopsis unicellular green algae *Chlamydomonas reinhardtii*, which possesses a simpler autophagic machinery compared to vascular plants, thus providing a new insight into ATG8 isoform-specific autophagy features in plants.

## Results

### *Expression of ATG8E ΔC restores accumulation of vacuolar puncta in ATG4-deficient Arabidopsis*

To identify the specific stage in the process of plant autophagosome formation where ATG8 delipidation plays a crucial role, we produced ATG8-based autophagosomal fluorescent markers in the wild-type (WT) and ATG4-deficient (*atg4a/b*) backgrounds of the vascular plant model organism *Arabidopsis thaliana*. Arabidopsis genome codes for nine orthologs of ATG8, referred to as isoforms ATG8A - ATG8I[14]. Since the ATG8E isoform has been previously successfully used as a marker for autophagic activity in Arabidopsis[15,16], we implemented it for this study as well. We generated stable Arabidopsis lines expressing three variants of EosFP-tagged ATG8E: a full length ATG8, a G/A lipidation-deficient mutant with a critical Gly residue substituted to Ala, and ATG8 ΔC, a truncated protein lacking the C-terminal peptide that would normally mask the critical Gly residue from lipidation (**Fig.1B** and **C**). When expressed in the *atg4a/b* background, ATG8 ΔC can efficiently form the ATG8–PE adduct anchored in the nascent autophagosomal membranes, however the latter cannot be delipidated in the absence of ATG4 activity.

The seedlings of the established marker lines were simultaneously treated with the autophagy-inducing compound AZD8055 (AZD), and with the compound concanamycin A (ConA) which increases vacuolar pH resulting in deactivation of hydrolases and therefore preservation of the autophagosomes delivered to the plant vacuoles[17]. Expectedly, upon upregulation of autophagy in the WT plants, full-length ATG8E was incorporated into autophagosomes and delivered to the vacuoles, where it was detectable in the form of fluorescent puncta (**Fig. 1D, Fig. S1**). The same marker remained dispersed throughout the cytoplasm in the *atg4a/b* background upon upregulation of autophagy, confirming the critical importance of ATG4-dependent processing for the ATG8's involvement in autophagosome formation. Lower intensity puncta were observed in the vacuoles of WT cells expressing the G/A mutant of ATG8, indicating that it might be taken up from the cytoplasm as a cargo. Such puncta were not observed in the vacuoles of *atg4a/b* cells, corroborating the lack of autophagic activity in this genetic background. Surprisingly, the truncated version, ATG8E ΔC, was observed in the vacuolar puncta of both WT and *atg4a/b*, indicating potential autophagic activity in the absence of ATG8 delipidation.

Given the unexpected nature of the observation described above, we found it necessary to confirm that the *atg4/b* mutant background used for this study is indeed ATG4-deficient. For this, we performed a thorough verification of the plants using genotyping, RT-PCR followed by an *in planta* ATG8-cleavage assay. The results of these assays confirmed the presence of the expected T-DNA insertions disrupting *ATG4A* and *ATG4B* genes (**Fig. S2A**), leading to the loss of the corresponding transcripts (**Fig. S2C**) and, subsequently, to the loss of ATG4 proteolytic activity (**Fig. S2D** and **E**).

### *Formation of plant autophagosomes and their delivery to the vacuole do not depend on ATG8 delipidation*

To verify that the observed EosFP-positive puncta were indeed autophagosomes and autophagic bodies labelled with the EosFP–ATG8–PE adduct, we expressed EosFP–ATG8E ΔC in the background lacking ATG8 lipidation activity, i.e. knockout of *ATG5* gene[18]. Transgenic plants expressing the truncated version of ATG8E were subjected to AZD/ConA treatment prior to imaging the root and shoot epidermal cells. Upon treatment, marker localized to vacuolar puncta in the WT and *atg4a/b*, but not in the *atg5* plants, confirming that punctate localization of the marker was dependent on ATG8 lipidation and therefore represented autophagosomal structures (**Fig. 2A**). Quantification of puncta revealed wild-type-like level of autophagic bodies accumulation in the vacuoles of *atg4a/b* cells, indicating reconstituted autophagic activity in the absence of the ATG8-delpidation step (**Fig. 2B**). We confirmed that this phenomenon was not specific to the early developmental stages of Arabidopsis and showed that accumulation of autophagic bodies was occurring in the adult plants as well by performing similar treatment on true leaves (**Fig. S3A** and **B**).

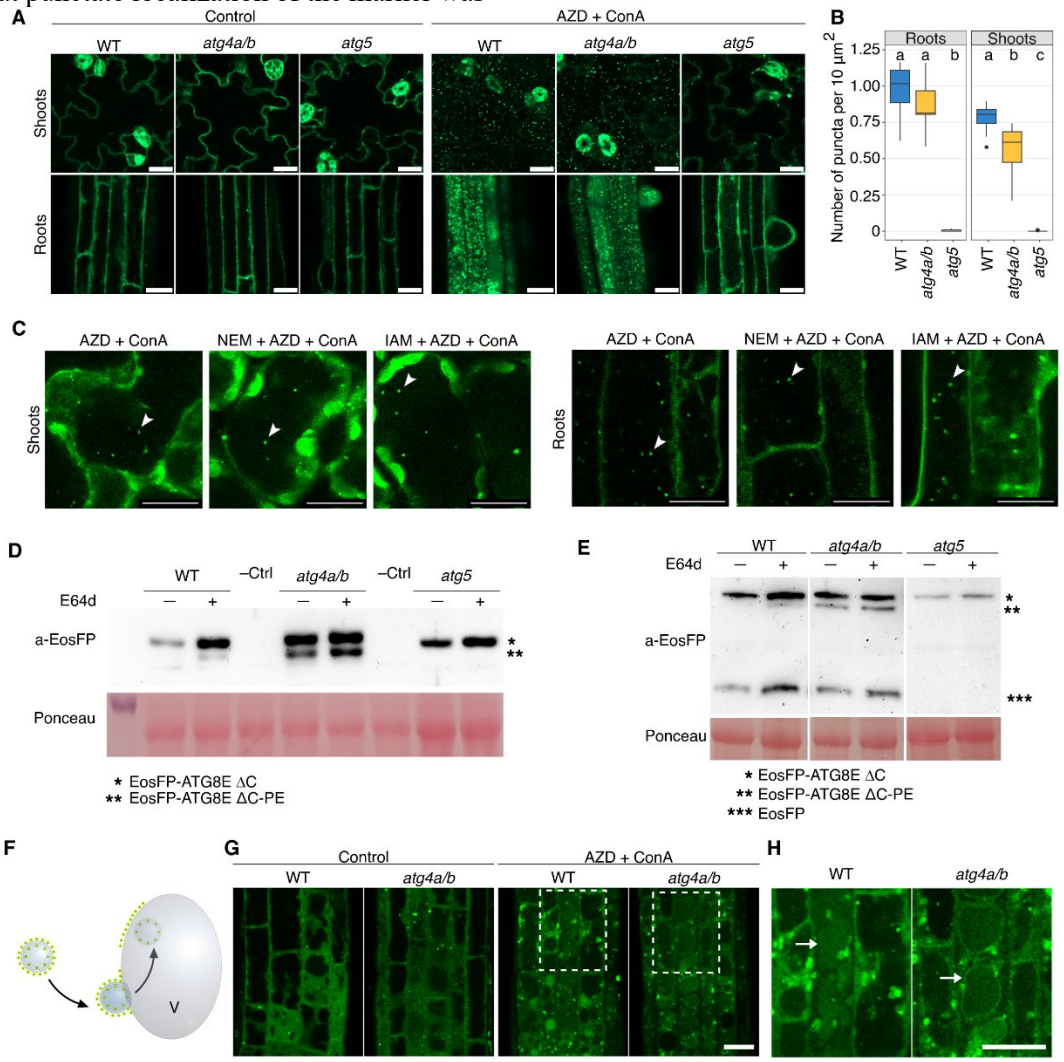


**Figure 2. Delipidation of ATG8E is dispensable for autophagosome formation and their delivery to the vacuoles.**
**A.** Confocal microscopy images of root and shoot epidermal cells of 7-days-old Arabidopsis seedlings expressing EosFP-ATG8E ΔC in WT, ATG4- or ATG5-deficient backgrounds. Seedlings were incubated under control conditions or subjected to AZD/ConA treatment. Scale bars, 20 µm.
**B.** Quantification of puncta per vacuolar area for the samples illustrated in **A**. Tukey's HSD test was performed for each plant organ individually, $n = 40$ for shoots and $n = 29$ for roots. Groups that do not differ are annotated by the same letter ($\alpha = 0.05$). Boxes indicate interquartile region (IQR); median is indicated by a horizontal line; whiskers represent range within 1.5 IQR; outliers are represented by a filled circle. The chart shows representative results of one out of two experiments.

**C.** Confocal microscopy images of EosFP–ATG8E ΔC expressed in mesophyll cell of WT Arabidopsis true leaves (left) or roots of 10 days old seedlings (right) treated with AZD/ConA in the absence or presence of irreversible cysteine protease inhibitors (1mM IAM or 10 mM NEM). Images for leaves were taken at 24 h of treatment, while roots where imaged after 4h of treatment. Time-lapse data confirming that the observed puncta are indeed freely in the vacuoles of leaves is available in the Movie S1.

**D.** Detection of EosFP in the protein extracts of seedlings treated with AZD/ConA and E64d (illustrated in **Fig. S3C and D**). Ponceau S staining was used as a loading control. –Ctrl, negative control (extract of a WT plant with no transgene). Western blot reveals accumulation of the EosFP–ATG8E ΔC–PE in ATG4-deficient background or in WT upon E64d treatment.

**E.** EosFP cleavage assay performed on the same material used for **E** shows no decrease in autophagic activity in the samples accumulating ATG8–PE.

**F.** Schematic representation of EosFP signal accumulation on the tonoplast upon its fusion with EoSP–ATG8E ΔC–decorated autophagosomes in the absence of ATG8-delipidation activity.

**G.** Confocal microscopy images of root epidermal cells expressing EosFP–ATG8E ΔC and showing accumulation of tonoplastic EosFP signal in ATG4-deficeint background upon upregulation of autophagy. Scale bar, 20 μm.

**H.** Zoomed-in images shown in **D** with adjusted contrast. Scale bar, 20 μm.

Next, we corroborated the results obtained *via* genetic manipulation of ATG4 by using chemical inhibitors of ATG4 activity. For this, 10-days-old seedlings and one-month-old plants expressing EosFP-ATG8E ΔC in the WT background were treated with AZD and ConA supplemented with iodoacetamide (IAM) or N-ethylmaleimide (NEM), chemical compounds previously shown to irreversible inhibit ATG4 activity[19–21]. Neither IAM nor NEM treatment prevented accumulation of autophagic bodies in the vacuoles of roots or shoots (**Fig. 2C; Movie S1**). Due to the strong cytotoxicity of these chemical compounds we decided to adhere to the use of genetic mutants for the future *in planta* experiments. Additionally, we tested another inhibitor of cysteine proteases, E64d which was suggested to not impact ATG4 activity but potentially stabilize autophagic bodies in the lytic compartment[22]. Accordingly, we did not observe a significant difference between WT and *atg4a/b* mock- or E64D-treated plants expressing EosFP–ATG8E ΔC (**Fig. S3C** and **D**). Western blot detection of the EosFP–ATG8 in the plants subjected to AZD/ConA treatment with or without E64d revealed accumulation of the ATG8–PE adduct in the ATG4 deficient background independently on the treatment. However, treatment with E64d rendered ATG8–PE detectable in the WT protein extracts, most probably due to the better stability of the adduct under these conditions. The ATG8–PE band was not detectable in the protein extracts of *atg5*, consistent with the lack of ATG8-lipidating activity in this mutant (**Fig. 2D**).

A study carried out in yeast revealed an APEAR motif (ATG8–PE association region) responsible for ATG4 recruitment to the lipidated form of ATG8 during autophagosome maturation[23]. Intriguingly, the APEAR motif is conserved in the ATG4B but not in the ATG4A Arabidopsis ortholog[8], indicating potential functional diversification of these orthologs in ATG8 processing. We tested if delipidation efficacy is reduced in the single *ATG4B* knockout. For this we crossed *atg4a/b* and WT plants expressing EosFP–ATG8E ΔC and performed Western blot detection of the tagged ATG8 in the young (2-weeks-old) and older (6-weeks-old) plants. Surprisingly, delipidation was significantly reduced in both *atg4a* and *atg4b* single gene knockouts (**Fig. S4**). These results demonstrate that while the proteolytic activity required for C-terminal processing of ATG8 can be efficiently executed by a single ATG4 (**Fig. S2D**), the delipidating activity of Arabidopsis ATG4s is significantly less efficient and requires expression of both genes. Notably, the single knockouts *atg4a* and *atg4b* do not have autophagy-deficient phenotypes[9,24], despite accumulating a significant amount of ATG8–PE (**Fig. S2D**). This observation is in agreement with the other results pointing towards ATG8 delipidation being dispensable for plant autophagy.

To corroborate reconstitution of autophagic activity in the absence of ATG8 delipidation, we deployed a modified version of the GFP cleavage assay[22], involving detection of EosFP–ATG8 processing upon induction of autophagy with AZD/ConA/E64d treatment. The assay demonstrated efficient processing of the fusion protein and accumulation of free EosFP in the plants expressing EosFP–ATG8E ΔC in the WT

and *atg4a/b*, but not in the *atg5* background (**Fig. 2E**), thereby corroborating restored autophagic activity in the absence of ATG8 delipidation.

We hypothesized that lack of ATG8-delipidating activity would result in a large number of EosFP–ATG8E ΔC-decorated autophagosomes fusing with the vacuolar membrane, which should eventually yield fluorescent labelling of the tonoplast (**Fig. 2F**). Indeed, upregulation of autophagy caused accumulation of tonoplastic EosFP signal in the *atg4a/b*, but not in the WT cells (**Fig. 2G and H)**.

In summary, these results confirm the expected accumulation of the lipidated ATG8–PE in the absence of delipidating activity and demonstrate the unexpected: normally-functioning autophagosome formation and delivery to the vacuole under these conditions.

### *ATG8 delipidation-independent autophagy restores wild-type like stress tolerance in the atg4a/b.*

We confirmed WT-like formation of plant autophagosomes in the absence of ATG8 delipidation. However, it still remained a question whether such autophagosomes can carry out the intended function. To test this, we assessed the stress tolerance of *atg4a/b* plants expressing EosFP–ATG8E ΔC under macronutrients-deprived conditions which would rely on autophagic activity[1,3] (**Fig. 3A-F**).

We performed uninterrupted time-lapse imaging of seedlings under nitrogen-deprived (–N) and carbon-deprived (–C) conditions. For this, seeds of WT, *atg4a/b* and *atg5* plants expressing EosFP–ATG8E ΔC were plated on standard 0.5xMS growth medium, and on growth media depleted of either nitrogen or sucrose. Plates were photographed every hour for 7 days using a SPIRO imaging platform[25]. For –C starvation induction, imaging was performed in the dark growth chamber using SPIROs green LED for illumination during image acquisition, to prevent photosynthetic carbon assimilation. We observed a stagnated root growth in autophagy-deficient plants (*atg4a/b* and *atg5*) under either of the macronutrients-deprived condition (illustrated in **Fig. 3A-C**; time-lapse movies showing complete plates are available in **Movies S2** and **S3**). Expression of EosFP–ATG8EΔC in the WT background did not have a discernible effect on root growth, however it reconstituted wild-type-like root growth in the *atg4a/b* background, revealing functional autophagic activity in these plants. No such effect was observed in the *atg5* plants expressing EosFP–ATG8E ΔC.

Similar to root phenotyping, assessment of seedlings shoot viability under the same stress conditions revealed restored stress-tolerance in the *atg4a/b* upon expression of ATG8E ΔC (**Fig. 3D-F**). Uncropped images of plates with plants used in these experiments are shown in **Fig. S5**.

Finally, we phenotyped the transgenic plants at the later developmental stages. Plants were grown in soil under long day conditions to detect the early senescence phenotype typical for autophagy-deficient Arabidopsis plants (**Fig. 3G and H**)[9]. Consistent with the above-described phenotyping assays, we could observe alleviation of the early senescence phenotype in the *atg4a/b* plants expressing EosFP–ATG8E ΔC.

In summary, the phenotypic assessment of stress-tolerance of the photosynthetic plant organs and of roots, carried out across developmental stages of Arabidopsis indicate that autophagic structures formed in the absence of ATG8 delipidation correspond to fully functional autophagosomes.

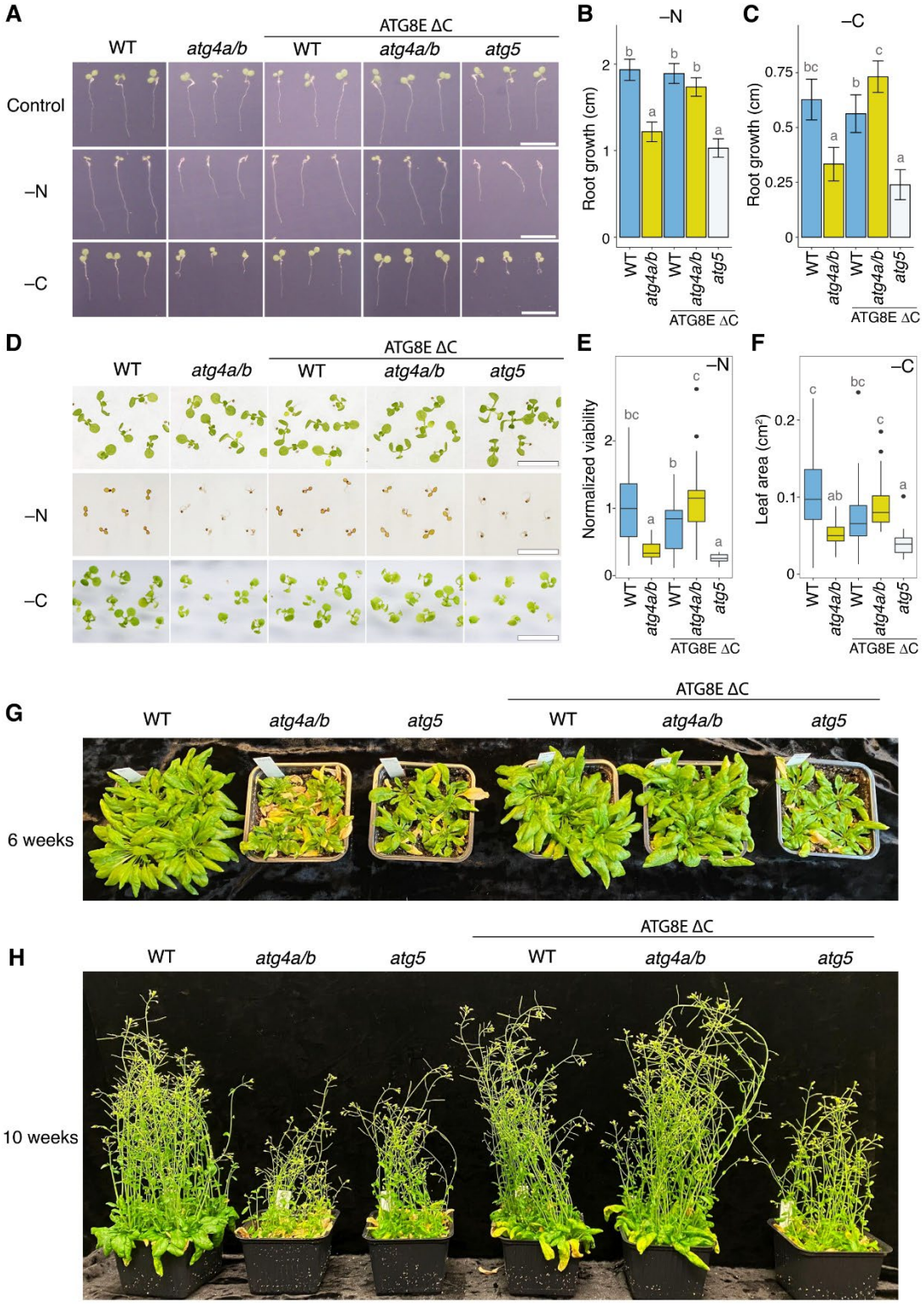


**Figure 3. Expression of ATG8E ΔC alleviates autophagy-deficient phenotypes of *atg4a/b***

**A**. Examples of Arabidopsis seedling roots phenotyped using SPIRO under control, nitrogen-depleted (–N), and carbon-depleted (–C) conditions. Normal root growth under nutrient-depleted conditions is restored in *atg4a/b* seedlings expressing ATG8E ΔC. In total, 997 biological replicates were phenotyped under –N and –C conditions in seven independent experiments.

**B**. Quantification of seedling root length on the 4$^{th}$ day after germination when grown under –N conditions, as illustrated in panel **A** (middle row). Boxes indicate interquartile region (IQR); median is indicated by a horizontal line; whiskers represent range within 1.5 IQR; outliers are represented by solid a filled circle. The chart represents combined data from two independent experiments (n = 364). Root growth was analyzed by fitting a mixed-effect second-order polynomial

model to the time-resolved root length data obtained by the SPIRO root growth assay. Letters signify all-pairwise comparisons, where treatments sharing the same letter do not differ at the α = 0.05 level. Error bars indicate 95% confidence interval.

**C**. Quantification of seedling root growth during four days of recovery following four days of carbon depletion, as illustrated in panel **A** (bottom row). Boxes indicate interquartile region (IQR); median is indicated by a horizontal line; whiskers represent range within 1.5 IQR; outliers are represented by solid a filled circle. The chart represents combined data from two independent experiments, *n* = 283. Root length was analyzed and visualized as in **B**.

**D**. Examples of Arabidopsis seedling shoot phenotypes under control, nitrogen-depleted (–N), and carbon-depleted (–C) conditions. Photos of complete plates are shown in **Fig. S4**.

**E**. Viability of Arabidopsis seedlings grown on –N medium illustrated in **D** (middle row) was estimated by shoot chlorosis. Phenotyping was performed in two independent experiments. The chart summarizes data from a single experiment (*n* = 157). The upper and lower edges of boxes indicate upper and lower quartiles of the data, the middle line indicates the median, and the whiskers extend to data points within 1.5 * interquartile range (IQR). Dots indicate data points outside 1.5 * IQR. Tukey's HSD test, shared letters indicate no difference at the α = 0.05 level.

**F**. Efficacy of recovery after carbon-depletion illustrated in **D** (bottom row) was estimated by measuring the leaf area/seedling at the end of a one-week-long recovery after seven days of carbon depletion. The experiment was performed twice. Chart shows representative data from one experiment (*n* = 160). Results were analyzed and visualized as in Panel **E**.

**G**. Rosette phenotype of 6 weeks old plants grown under long day conditions show a typical attribute for autophagy-deficient plants, early onset of senescence, in the *atg4a/b* and *atg5* plants, and lack thereof in the *atg4a/b* plants expressing ATG8E ΔC protein.

**H**. Inflorescence phenotype imaged one month later for the same plants as shown in **G**.

### *Arabidopsis ATG8 isoforms differ in their capacity to carry out autophagic flux*

Two out of nine Arabidopsis ATG8 isoforms, ATG8H and ATG8I, lack the C-terminal peptide and therefore do not require processing by ATG4 for their lipidation. It is conceivable that these two isoforms can be readily lipidated and used for biogenesis of autophagosomes in the *atg4a/b* mutant (**Fig. 1A** and **B**, **Fig. 4A**). Reflecting upon our discovery that autophagy can be reestablished in the ATG4-deficient background through expression of the truncated ATG8E, we wondered why the naturally truncated ATG8 isoforms do not similarly reinstate autophagosome formation in *atg4a/b* plants. We considered two plausible explanations: (i) the sum amount of ATG8H and ATG8I (which would correspond to the total amount of ATG8 available for lipidation in *atg4a/b*) is much lower than the sum amount of all isoforms ATG8A-ATG8I available for lipidation in the WT background and might not be sufficient for normal autophagosome biogenesis; (ii) ATG8H and ATG8I isoforms play specific roles in plant autophagy that do not include participation in autophagosome biogenesis, e.g. sequestration of specific cargo. Indeed, ATG8H and ATG8I isoforms show higher protein sequence similarity with animal ATG8 orthologs compared to ATG8A-G (**Fig. S6A** and **B**)[14], suggesting a potential functional diversification of these isoforms.

To test these hypotheses, we selected two strongest expressed ATG8 isoforms, one with and one without C-terminal peptide, ATG8F and ATG8I, respectively (**Fig. 4B**). We generated fluorescently labelled fusions of these isoforms and expressed them transiently from a strong native Arabidopsis promoter (*APA1*[26]) in WT, *atg4a/b* and *atg7* cells, using the latter as a negative control deficient in the ATG8 lipidation activity. Upon induction of autophagy, we could observe the expected accumulation of autophagic body-like structures in the vacuoles of WT cells expressing either of the ATG8 isoforms, and lack thereof in the vacuoles of *atg7* mutants (**Fig. S6C**). Intriguingly, overexpression of ATG8I in the *atg4a/b* background seemed to have reconstituted accumulation of puncta in this background, thus supporting our first hypothesis that the amount of ATG8 available for lipidation might be the limiting factor in *atg4a/b* autophagy. As expected, ATG8F overexpression in the same cells did not reconstitute autophagosome biogenesis.

To enable an in-depth investigation of this finding using biochemistry and phenotyping assays, we generated stable transgenic lines overexpressing GFP-fusions of the same ATG8 isoforms under the control of a strong viral promoter. Detection of autophagic bodies in the true leaves of these plants confirmed the results obtained in the transient expression system: indeed, overexpression of ATG8I was sufficient to reconstitute accumulation of autophagic

bodies in the vacuoles of *atg4a/b* upon AZD/ConA treatment (**Fig. 4C**). The GFP-cleavage assay on protein extracts from the plants overexpressing GFP–ATG8 isoforms further confirmed autophagic flux present in the *atg4a/b* overexpressing the natively truncated ATG8I isoform (**Fig. 4D**). Intriguingly, detection of the lipidated and non-lipidated adducts of ATG8 in the protein extracts from plants overexpressing ATG8F and ATG8I isoforms revealed accumulation of the ATG8I–PE not only in the *atg4a/b* but also in the WT background (**Fig. 4E**), suggesting a decreased affinity of ATG4 towards this isoform.

The decreased efficacy of GFP–ATG8I cleavage in *atg4a/b* background in comparison to the WT (**Fig. 4D** and **E**) suggested that our second hypothesis might also be correct, and that ATG8I cannot fully reconstitute normal autophagosome formation. To test this, we compared the number of puncta formed in the Arabidopsis root cells overexpressing ATG8E ΔC, ATG8F, or ATG8I upon upregulation of autophagy. For this, Arabidopsis seedlings overexpressing either of the ATG8 isoforms in the WT, *atg4a/b*, or *atg5* background were subjected to AZD/ConA treatment for 24 h followed by confocal laser scanning microscopy (CLSM) imaging (**Fig. 4F**). Quantification of the puncta on the obtained micrographs revealed no significant difference between puncta density in the WT and *atg4a/b* overexpressing ATG8I (**Fig. 4G**), indicating normal rate of autophagosome formation and their delivery to the vacuole. However, it did not escape our notice, that the size of the GFP–ATG8I-positive puncta differed in the WT and *atg4a/b* cells. Quantification of the puncta size distribution showed that indeed, autophagic bodies formed in the *atg4a/b* cells overexpressing ATG8I were significantly smaller in comparison to autophagic bodies observed in the vacuoles of WT cells overexpressing the same isoform (**Fig. 4H**).

Next, we tested if the decreased size of autophagic bodies in the ATG8I overexpressing *atg4a/b* plants was impacting efficacy of autophagic activity. We subjected seedlings to nitrogen starvation and measured elongation efficacy of their roots using SPIRO time-lapse images (**Fig. 4I** and **J**). Noteworthily, the overexpression of ATG8I did not rescue the stagnated root growth phenotype of *atg4a/b*, indicating that smaller autophagosomes in these cells were not sufficient to cope with scarcity of exogenous nitrogen. Surprisingly, we also observed a decreased root elongation in the WT plants overexpressing ATG8I (**Fig. 4I** and **J**). Considering that the puncta quantification experiments (**Fig. 4F** and **G**) were performed using AZD as a trigger for autophagy, while root phenotyping was done under –N conditions (**Fig. 4I** and **J**), we decided to test if the overexpression of ATG8I has a different effect on WT depending on the stress conditions. For this, we compared autophagic bodies density and size upon AZD, –N and –C treatments (**Fig. S7**) using overexpression of ATG8E ΔC, which caused no discernible phenotype in the WT in the previous experiments, and overexpression of ATG8I that caused decreased tolerance to nitrogen depletion in WT. In agreement with our previous observations, ATG8E ΔC overexpression in the WT and *atg4a/b* backgrounds yielded similar autophagic bodies density and size under all three stress conditions, while overexpression of ATG8I isoform in the *atg4a/b* yielded smaller autophagic bodies (**Fig. S7A, C** and **D**). Surprisingly, the size of autophagic bodies in the WT cells overexpressing the ATG8I isoform was significantly smaller under –N conditions when compared to the puncta size in the same transgenic line under –C or AZD treatment (0.51 $\mu m^2$ under –N vs 0.76 $\mu m^2$ under –C, or 0.69 $\mu m^2$ under AZD, Tukey's HSD test $p$-value <0.001; **Fig. S7A** and **D**), thereby explaining the observed stunted root growth on nitrogen-depleted medium. The autophagic flux rate under the three stress conditions was additionally confirmed using GFP-cleavage assay (**Fig. S7B**).

Since ATG8I overexpression did not impact the size of autophagic bodies in the WT cells under AZD and –C conditions, it can be deduced that excessive amount of this isoform is unlikely to cause premature phagophore closure and probably impacts autophagosome size by shifting autophagy selectivity towards cargo.

Interestingly, when plants were grown under favorable long day conditions in soil, WT overexpressing ATG8I showed no discernible phenotype, while *atg4a/b* plants overexpressing the same isoform grew more fit than autophagy-deficient knockouts (**Fig. 4K**). These observations suggest that ATG8I overexpression can rescue autophagy of the *atg4a/b* knockout to a level that is sufficient for WT-like plant fitness under

favorable conditions, and that toxic effects of ATG8I overexpression in the WT is specific for certain types of stresses, including –N.

In summary, we demonstrated that the autophagy-deficient phenotype of *atg4a/b* is caused by insufficient amount of the correct ATG8 isoform available for lipidation during autophagosome formation. We showed that overexpression of the natively truncated ATG8I isoform is sufficient to reconstitute normal rate of autophagosome formation and their delivery to the vacuole but yields autophagosomes twice smaller than formed when artificially truncated ATG8E isoform is expressed in the same background. Furthermore, overexpression of the natively truncated ATG8I isoform undermines tolerance of WT plants to nitrogen deprivation, possibly by shifting autophagy selectivity to the one unfavorable under such conditions.

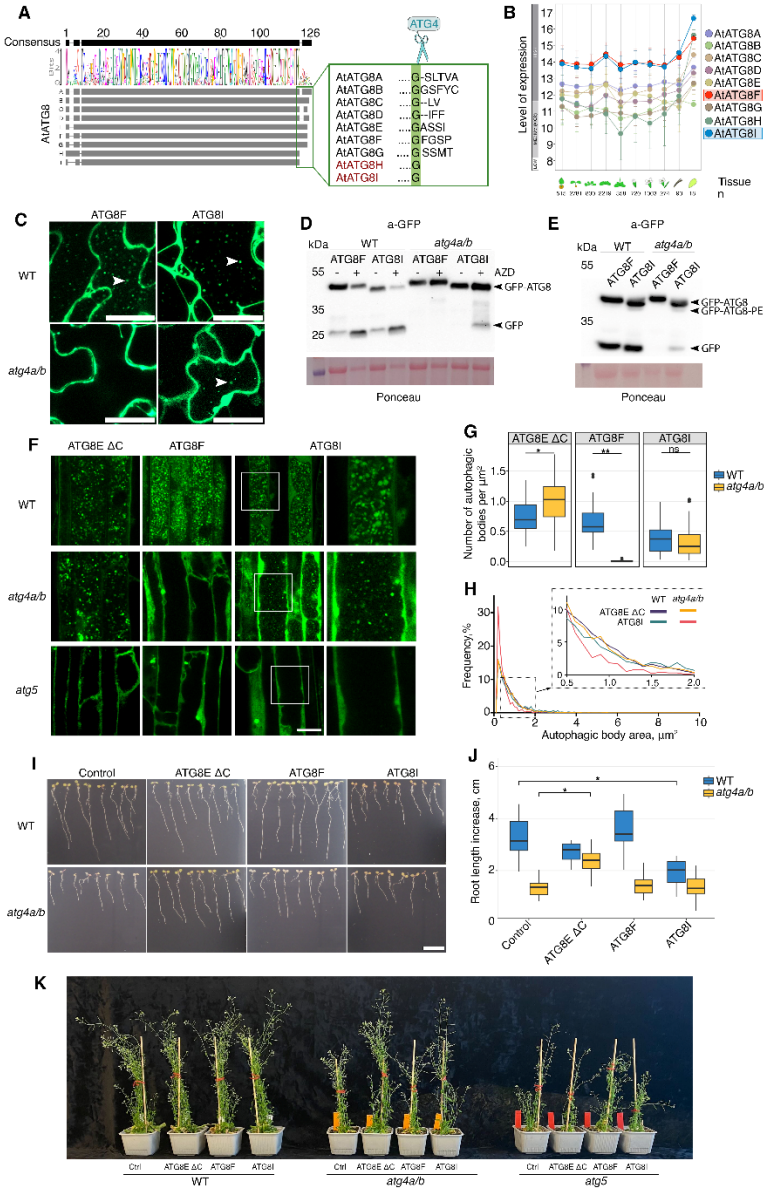


**Figure 4. Arabidopsis ATG8 isoforms differ in their capacity to carry out autophagic flux.**

**A.** Schematic representation of ClustalW protein alignment of the nine Arabidopsis ATG8 isoforms. The inset shows ATG8 C-terminal sequences containing the Gly residue which is critical for lipidation. Notably, ATG8H and ATG8I do not possess the C-terminal peptide and have the critical Gly readily exposed.

**B.** GENEVESTIGATOR data on organ-specific expression of all nine ATG8 isoforms of Arabidopsis. ATG8F (red rectangle) and ATG8I (blue rectangle) isoforms are expressed at the highest level in all tissues.

**C.** Confocal microscopy images showing accumulation of autophagic bodies in the vacuoles of leaf epidermal cells stably expressing GFP-tagged ATG8F or ATG8I in WT or *atg4a/b*. Leaves were infiltrated with AZD/ConA 24 h prior to imaging. White arrowheads point at autophagic bodies. Scale bars, 25 µm.

**D.** GFP cleavage assay performed on the transgenic lines illustrated in **C**, showing restored accumulation of free GFP in the *atg4a/b* plants expressing GFP–ATG8I. Autophagy was induced by infiltrating leaves with AZD 24 h prior to sampling.
**E.** Western blot detection of GFP in AZD-treated samples shown in **D** separated on the gel containing 6 M urea to discern lipidated from non-lipidated forms of ATG8 confirms accumulation of the lipidated ATG8I. The panel shows results representative for two independent experiments.
**F.** Confocal microscopy images showing accumulation of autophagic bodies in root epidermal cells of seedlings expressing three isoforms of Arabidopsis ATG8 (ATG8E ΔC, ATG8F and ATG8I) in the WT, ATG4- or ATG5-deficient backgrounds. Seven days old Arabidopsis seedlings were subjected to AZD/ConA treatment for 24 h prior to imaging. Scale bars, 20 µm.
**G.** Quantification of autophagic bodies in vacuoles of cells illustrated in **F**. Welch's t-test, $n = 337$. *, $p < 0.05$; **, $p < 0.01$; ns, not significant. Boxes indicate interquartile region (IQR); median is indicated by a horizontal line; whiskers represent range within 1.5 IQR; outliers are represented by a filled circle.
**H.** Size distribution of autophagic bodies in the samples illustrated in **F** and quantified in **G**. The inset shows a magnified portion of the chart visualizing the higher frequency of smaller autophagic bodies present in the vacuoles of *atg4a/b* plants expressing ATG8I.
**I.** Root growth phenotype of 12-days-old seedlings incubated for 7 days on nitrogen depleted medium. Expression of native truncated ATG8I isoform is not sufficient to alleviate the autophagy-deficient phenotype of *atg4a/b*. Seedlings were grown for 4 days on standard 0.5xMS medium, checked for GFP signal, then transferred onto –N medium plates to be imaged for 7 days.
**J.** Quantification of the increase in root length of the seedlings after 7 days growth on the –N medium (illustrated in **I**). The experiment was performed three times. Boxes indicate interquartile region (IQR); median is indicated by a horizontal line; whiskers represent range within 1.5 IQR; outliers are represented by solid a filled circle. The chart shows representative data from one experiment. Dunnett's tests were performed for WT and *atg4a/b* separately, comparing each genotype against the control sample ($n$ =128). *, $p < 0.0001$.
**K**. Phenotypes of two months old plants grown in soil under long day conditions. Photos show plants with representative phenotypes, the experiment was performed twice using four biological replicates for each genotype. Ctrl, a not transformed plant of the corresponding genotype; ATG8E ΔC, ATG8F and ATG8I, overexpression of the fluorescent fusion of the corresponding ATG8 isoform.

### *ATG8 delipidation is critical for autophagy in a green alga*

To investigate whether delipidation of ATG8 is dispensable for autophagy in other lineages, we conducted experiments on the unicellular green alga, *Chlamydomonas reinhardtii*, a close relative of plants. *Chlamydomonas* genome encodes single genes for the core ATGs, making it a much simpler model for autophagy research compared to Arabidopsis. Its ATG8 protein has the C-terminal peptide, which necessitates the ATG4-dependent processing step prior to ATG8 lipidation (**Fig. 1A** and **B**). Therefore, we generated a truncated version of *Chlamydomonas reinhardtii* ATG8, CrATG8 ΔC, which had the critical C-terminal Gly exposed and could be lipidated in the absence of ATG4 activity but would depend on it for the delipidation.

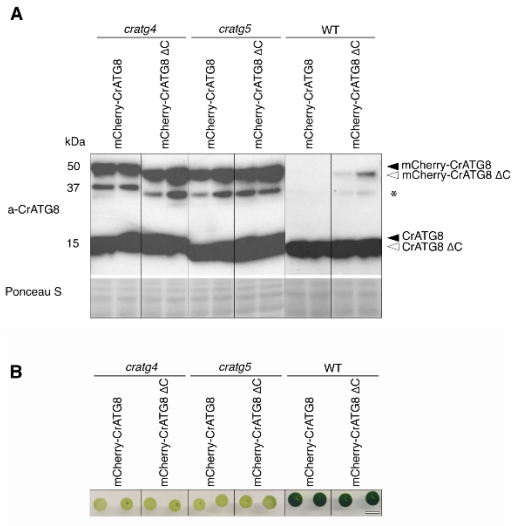


**Figure 5. Delipidation of ATG8 is critical for autophagy in *Chlamydomonas reinhardtii*.**
**A.** Western blot detection of endogenous ATG8 and mCherry–CrATG8 transgene expression in the WT, *cratg4,* and *cratg5* backgrounds. Ponceau S staining was used as a loading control. The cells were grown in the liquid TAP medium under standard conditions and harvested at a density of 1-2×107 cells $ml^{-1}$. *, a putative product of autophagy-independent proteolytic processing of mCherry-CrATG8.
**B.** Senescence phenotype of the transgenic *Chlamydomonas* lines grown on the TAP medium for 40 days. Light color of colonies indicates nutrient deficiency sensitivity caused by dysfunctional autophagy. Scale bar, 1 cm.

First, we generated *cratg4* and *cratg5* autophagy-deficient mutants in the UVM4 background (**Fig. S8**) and complemented them with mCherry-tagged full-length CrATG8 or CrATG8 ΔC. Immunoblot analysis of the established transgenic lines showed a good expression level of both transgenes in the autophagy knockout lines (**Fig. 5A**). A lack of autophagy elicits early senescence phenotype, especially under nutrient-scarce conditions[27,28]. Therefore, we assessed the functionality of the autophagic pathway in the established strains by assessing their rate of senescence. We cultivated the strains in TAP medium for 40 days and monitored the degree of their chlorosis while they were gradually depleting nutrients from the medium (**Fig. 5B**). Expectedly, *cratg5* mutants complemented with full-length or truncated ATG8 but still deficient in ATG8 lipidation exhibited chlorosis associated with the early senescence phenotype, while WT cells remained dark green under the same conditions (**Fig. 5B**). Notably, the early senescence phenotype in the *cratg4* mutant was not rescued by the expression of the truncated ATG8 version (**Fig. 5B**). This observation suggests that, in contrast to results obtained for vascular plants, but in accordance with observations made in yeast and mammals, ATG8 delipidation plays a crucial role in autophagy in the green alga.

## Discussion

In this study we demonstrate that ATG8 delipidation is dispensable for autophagy in the vascular plant *Arabidopsis thaliana*, which belongs to the Streptophyta lineage. However, it is of crucial importance for autophagy in the unicellular green alga *Chlamydomonas reinhardtii*, which is part of the Chlorophyta lineage. The specific evolutionary adaptations that rendered delipidation dispensable have yet to be uncovered.

Since ATG8 delipidation was previously reported to be crucial for autophagy in plants[9], as well as in yeast and animal cells[6,10,11], we considered it imperative to conduct a thorough verification of our surprising observation regarding the reconstituted autophagosome formation in the ATG4-deficient Arabidopsis. We employed a combination of mutagenesis, cell biology, biochemistry, and phenotyping assays to establish a robust foundation for future investigations aimed to elucidate the molecular mechanisms governing plant-specific maturation of autophagosomes possible in the absence of ATG8 delipidation.

Importantly, upon thorough evaluation, we determined that none of our results directly contradicts data presented in the study by Yoshimoto and colleagues[9]. The differences in our conclusions probably stem from serendipitous factors. For example, in our study we selected to test an artificially truncated ATG8E isoform which turned out to be more potent in enabling autophagic flux than the natively truncated ATG8I used by Yoshimoto and colleagues. Furthermore, our results clearly demonstrate that overexpression of GFP–ATG8I yields a lower autophagic activity in *atg4a/b* than in WT. Therefore, activity in *atg4a/b* might have fallen below the detection limit for the assay relying on the imaging of the diffuse GFP signal diluted in the vacuolar volume, implemented by Yoshimoto and colleagues. In our study we opted for imaging autophagic bodies represented by bright puncta of concentrated GFP signal, therefore increasing the chance of detecting even a weak autophagic activity.

Based on our observations, we propose that plant autophagosome maturation diversified into strategies dependent on and independent from ATG4 delipidating activity (**Fig. 6**). It is an intriguing question, how a critical step regulating autophagosome maturation became unnecessary in some eukaryotes. Noteworthily, the concept of "conserved step" in this context should be viewed with some caution: while disruption of ATG8 delipidation indeed halts autophagosome biogenesis in yeast and mammalian cells, it affects different stages of the process in these organisms[6,10,12,13], indicating inherent differences in why this step is critical for autophagy in various eukaryotes.

Autophagy was likely invented by the Last Eukaryotic Common Ancestor (LECA)[29] to maintain the newly acquired complex cell structures, such as organelles. During evolution of eukaryotes, autophagy has diversified to adapt to the various life strategies, mobility traits, nutrient requirements, and specific configurations of endomembrane trafficking systems observed in fungi, animals, plants and algae. For example, eukaryotes evolved different configurations of the lytic compartment — the final destination of

the autophagic pathway. The main lytic compartment of animal cells are compact and mobile lysosomes that upon upregulation of autophagy are co-trafficked together with autophagosomes transported to the fusion location (**Fig. 6**). The modest size of lysosomes and their importance for other cellular pathways, compels animal cells to regenerate these organelles after their fusion with autophagosomes in a process known as autolysosome recovery (ALR)[30]. Such a process has not yet been reported for fungal and plant cells, in which autophagosomes fuse with the large lytic vacuoles that often occupy most of the cell volume[1,3].

Notably, autophagosome biogenesis in yeast cells occurs in proximity to the vacuole, at the single phagophore assembly site[2] (**Fig. 6**). Consequently, once complete, autophagosomes fuse immediately with vacuoles. In contrast, autophagosomes in animal cells emerge at multiple locations, and are trafficked towards nuclei to fuse there with the perinuclearly translocated lysosomes[31]. Interestingly, plants' autophagic strategy seems to be somewhere in-between the yeast and animal solutions (**Fig. 6**). That is, autophagosomes form at multiple foci and are trafficked towards the immobile large lytic vacuole[3]. In view of these facts, it is conceivable that despite conservation of the core autophagic mechanisms, some molecular aspects of the pathway might significantly differ in vascular plants, algae, fungi and animal cells.

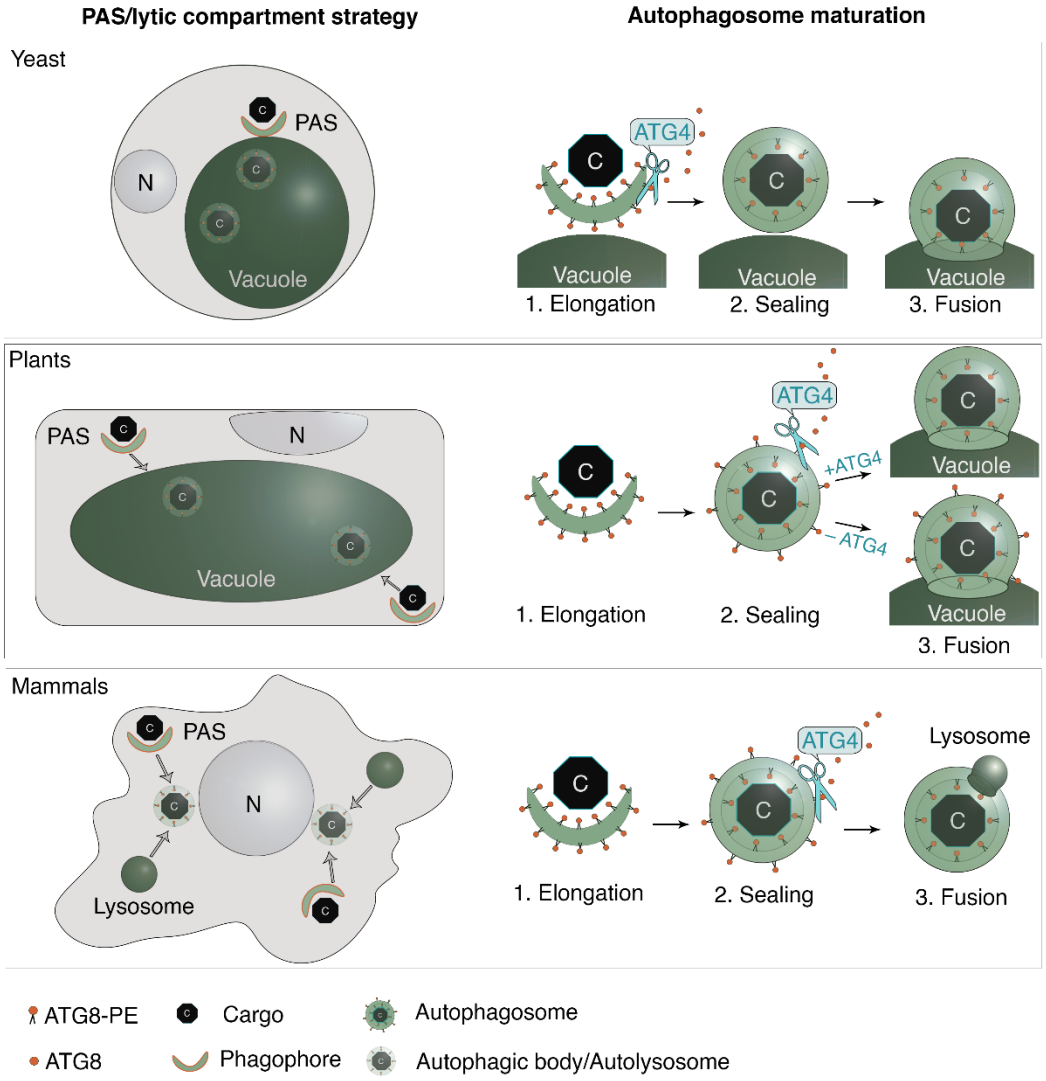


**Figure 6. Schematic representation of ATG8 delipidation importance for autophagy in the three eukaryotic kingdoms.**
ATG4-dependent delipidation of ATG8 is considered to be generally conserved in plants, animals and fungi. However, this process is critical for early steps of autophagosome maturation in yeast cells (phagophore elongation), while in mammalian cells the same delipidation step is critical for the later stage of autophagy (docking of complete autophagosomes to lysosomes). In this study we show that although ATG8 delipidation occurs in plants, it is dispensable for autophagy.

The different roles ATG8-delipidation plays in autophagosome maturation might be representative of autophagy adaptation to the various strategies for the lytic compartment (single large immobile vacuoles in plant and yeast cells *vs* numerous small motile lysosomes in animal cells), for phagophore assembly sites (single site in yeast *vs* numerous sites in animal and plant cells), and autophagosome trafficking towards the lytic compartment (autophagosome formation in the proximity to the vacuole in yeast, trafficking of autophagosomes towards immobile vacuole in plants, coordinated trafficking of autophagosomes and lysosomes to their meeting spot in mammalian cells).
C, cargo; N, nucleus.

ATG8 recruits other core ATG proteins to the growing phagophore. Subsequently, delipidation of ATG8 from maturing autophagosome was suggested to release PAS proteins prior to the fusion of the autophagosome with the lytic compartment thus preventing their unnecessary degradation[2]. Interestingly, such release of the core ATGs might be less critical for Arabidopsis autophagy. For instance, ATG1a was shown to be delivered to the vacuole together with autophagosomes[32]. Future studies identifying proteins decorating mature plant autophagosomes will help to elucidate how they are affected by ATG8-delipidation.

In higher eukaryotes, some of the ATG gene families expanded quite significantly[3,14,33]. For example, Arabidopsis has nine ATG8 and two ATG4 orthologs. The reasons behind ATG gene families expansion is not fully understood, but it is likely that functional diversification of ATG isoforms became necessary within the context of complex organisms. For instance, Zess and colleagues previously suggested a model according to which plant autophagosomes might vary in their ATG8 isoform content and consequently contain different cargo[34]. In the present study, we demonstrate drastic differences in the size of the autophagosomes formed with participation of ATG8F and ATG8I isoforms, as well as their impact on plant stress tolerance. In the future we plan to determine the differences in the content of the ATG8F- and ATG8I-specific autophagic bodies and explain their impact on plant stress tolerance.

Current evidence indicates that Arabidopsis ATG4 orthologs are redundant: Arabidopsis knockouts of single *ATG4* genes do not have autophagy-deficient phenotypes[9,24]. Furthermore, we demonstrated that either of the ATG4 proteases is sufficient for complete processing of ATG8 *in planta* (**Fig. S2D**). Intriguingly, we also revealed that efficient delipidation of ATG8 requires the presence of both ATG4 proteases (**Fig. S4**), indicating that the delipidating activity of ATG4s is significantly less efficient than their proteolytic activity, which might play a role in preserving the pool of ATG8–PE required during phagophore expansion. Similarly, highly efficient proteolytic activity and slower delipidation activity was reported to be characteristic for the mammalian ATG4s[12].

Interestingly, yeast ATG4 contains the N-terminal motif, APEAR, responsible for its association with ATG8–PE during delipidation step[8], while mammalian ATG4s were shown to associate with ATG8–PE via their C-terminal LIR motif[12]. It remains to be determined which of the predicted motives of Arabidopsis ATG4s is responsible for association with ATG8–PE. Yet, the APEAR motif is an unlikely candidate for it, as it is present only in the ATG4B, while both ATG4A and ATG4B partake in ATG8 delipidation (**Fig. S4**).

Here we report an additional intriguing observation of naturally truncated ATG8I isoform accumulating in its ATG8I–PE version in the WT upon upregulation of autophagy (**Fig. 4E**). This is quite uncharacteristic for plant ATG8s, as their lipidated adducts are notoriously difficult to detect in plant protein extracts[24]. Future studies will determine whether such accumulation is caused by the decreased affinity of ATG4 towards ATG8I. Such a loss of affinity is plausible because the natively truncated ATG8 isoforms do not require interaction with ATG4 for processing before lipidation, and their interaction with ATG4 for delipidation is dispensable for autophagy.

In conclusion, we discovered that in contrast to yeast, mammals and green algae, vascular plants do not require ATG8 delipidation for autophagosome maturation and delivery to a lytic compartment. In addition, our study provides a novel insight into the isoform-specific role of ATG8 in plant autophagy and lays foundation for the future research on the mechanism of plant autophagosome maturation.

## Competing interests

The authors declare no competing interests.

## Acknowledgments

This study was supported by grants from EU Horizon 2020 MSCA IF (799433 to EA Minina), Carl Tryggers Foundation (CTS 14 326 and 20:287 to EA Minina), The Swedish Research Council Formas (2017-00541 to PV Bozhkov and 2021-01812 to EA Minina), The Knut and Alice Wallenberg Foundation (2018.0026 to PV Bozhkov), DFG (CRC1101, TPA02 to K Schumacher), and Crops for the Future Research Program at the Swedish University of Agricultural Sciences.

## Materials and methods

### *Arabidopsis plant material and growth conditions*

All experiments were performed in Col-0 Arabidopsis accession (N1092). Autophagy-deficient mutants were described previously: *atg4a-2/atg4b-2*[35] (*atg4a/b* in this study), *atg5-1*[18](*atg5* in this study), *atg7-2*[36] (*atg7* in this study).

For cultivation on plates, Arabidopsis seeds were surface sterilized with bleach. In brief, seeds were agitated for 20 min in 10% bleach (Klorin, Sweden) water solution supplemented with 0.05% Tween-20, washed in four changes of sterile MQ water and plated on 0.5xMS medium, comprising 0.5xMS (*Duchefa*, ref. M0222); 10 mM MES (*Duchefa*, ref. M1503); 1% sucrose; pH 5.8; 0.8% Plant agar (*Duchefa*, ref. P1001). Plates were sealed with plastic wrap and incubated vertically under long day conditions: 16/8-hour light /dark cycle at PAR 150 µmol photons $m^{-2}$ $s^{-1}$, at 22°C.

S-Jord soil (Hasselfors, Sweden) was used to grow Arabidopsis plants in pots. Plants were incubated under long day conditions: 16/8-hour light /dark cycle at PAR 150 µmol photons $m^{-2}$ $s^{-1}$, at 22°C.

### *Chlamydomonas strains and growth conditions*

UV mutagenesis strain 4 (UVM4) capable of efficiently overexpressing foreign genes[37] was used as the WT background in this study. The *Chlamydomonas* cells were grown in tris-acetate-phosphate (TAP) medium at 23°C and a light-dark cycle (LD16:8). The cells were harvested at a density of 1-2×$10^7$ cells $ml^{-1}$ for immunoblot analysis or genomic DNA isolation.

### *Cloning of constructs*

Constructs for studies in Arabidopsis was generated using GreenGate[38] and Gateway (Invitrogen) cloning systems. For expression of recombinant ATG4 proteases we created constructs coding N-terminal GST fusions of the wild-type and catalytically inactive Arabidopsis ATG4 proteins. For this, ATG4A (AT2G44140) and ATG4B (AT3G59950) CDS were lifted from total cDNA of Arabidopsis thaliana using primers AM 417/418 and AM 419/420, respectively (Table S1). Active sites of ATG4A and ATG4B were mutated using QuikChange II Site-Directed Mutagenesis Kit (Agilent, 200523) and primer pairs AM 622/AM 623 and MA 624/625, respectively (Table S1). Amplicons were recombined with pDONR/Zeo vector using Gateway cloning system (Invitrogen). The resulting constructs AM 753 and AM 754 (Table S2) further recombined with pDEST15 (Gateway™, Invitrogen) to obtain AM 810-813 destination constructs (Table S2).

The constructs encoding EosFP–AtATG8E variants for expression in plants were generated using Gateway cloning system (Invitrogen). To clone full-length ATG8E, ATG8E G/A and ATG8E ΔC, the genomic sequence of ATG8E (*AT2G45170*) was lifted from the total genomic DNA of *Arabidopsis thaliana* using primers AM 475/476, AM 475/478 and AM 475/477, respectively (**Table S1**). Amplicons were recombined with pDONR/Zeo vector using Gateway cloning system (Invitrogen). The resulting constructs AM 655-657 (**Table S2**) were further recombined with pUBN EosFP[39] to obtain AM 661-663 destination clones (**Table S2**).

The constructs encoding EosFP–AtATG8A–CFP for expression in plants was generated by first fusing ATG8A gene with CFP CDS using overlay PCR. For this, ATG8A gene (*AT4G21980*) was lifted from the total genomic DNA of *Arabidopsis thaliana* using primers

AM 429/430, CDS of CFP was amplified from pGWB 661[40] (**Table S1**). The obtained amplicons were fused in a PCR with primers AM 431/AM 428 (**Table S1**) and the product was recombined with pDONR/Zeo vector using Gateway cloning system (Invitrogen). The resulting constructs AM 556 (**Table S2**) was further recombined with pUBN EosFP[39] to obtain AM 567 destination clone (**Table S2**).

The constructs encoding GFP–AtATG8F and GFP–AtATG8I fusion proteins for expression in plants were generated using GreenGate system, following the published instructionse[38]. pGGC ATGF (plasmid SH3, **Table S2**) and ATG8I (plasmid SH4, **Table S2**) modules were generated by recombining the pGGC0 module with the PCR products obtained on the total cDNA of *Arabidopsis thaliana* using primers SH PR 7/SH PR 8 and SH PR 9/SH PR 10, respectively (**Table S1**). pGGA 2x35S promoter (SH 117, **Table S2**) was produced by recombining the plasmid with the PCR product using primer pair SH PR 34/SH PR 35 (**Table S1**). The rest of the required modules were kindly provided by K. Schumacher's and A. Maizel's labs. The destination vectors AM 780 and AM 783 (**Table S2**) were obtained by recombining pGGZ004, SH 117, pGGB -E2GFP-GSL, SH 3 or SH 4, pGGD decoy, pGGE NosT and pGGF FAST Red pLB012.

SH 3 and SH 4 clones were also used to create construct expressing mScarlet-tagged ATGF and ATG8I, respectively (SH 17 and SH19, **Table S2**).

Cloning of constructs for experiments in *Chalmydomonas* was done using the modular cloning MoClo toolkit published by Crozet and colleagues[41]. CrATG8 (Cre16.g689650) and CrAT8 ΔC were amplified using primers ATG8_F and ATG8_R or ATG8 ΔC _R and genomic DNA as a template. Amplicons were cloned into the B5 module (L0 module) of thee MoClo system. Two L1 vectors were constructed using the following L0 modules: *PsaD* promoter (pCM0-016), *mCherry* gene (pCM0-067), the genomic sequence of *CrATG8* or *CrATG8* ΔC, and the *PsaD* terminator (pCM0-114). L2 level vectors were assembled with hygromycin resistance. The L2 level vectors were introduced into WT, *atg4* and *atg5* strains using the glass beads methods[42].

***Establishment of Arabidopsis transgenic lines***

Transgenic lines established for this study are listed in Table S3. WT, *atg4a/b* and *atg5* Arabidopsis plants were transformed using the standard floral dip method[43] and *Agrobacterium tumefaciens* strain GV3101. Transgenic plants were selected on the corresponding herbicide or, in case of FastRed selection marker, detecting the red fluorescence in the seeds using an upright epifluorescence microscope (Axioplan, Zeiss). Fluorescent signal in the seedlings was verified using CLSM (LSM800, Zeiss and SP8, Leica). Expression of the protein with the expected molecular weight was confirmed with a Western blot analysis. The presence of the T-DNA inserts in the knockout backgrounds was verified by genotyping (**Fig. S2**).

To obtain single *ATG4* knockout lines expressing EosFP–ATG8E ΔC or EosFP–ATG8A–CFP, we performed crosses between *atg4a/b* plants carrying the respective constructs and WT plants carrying the same constructs.

***Establishment of Chlamydomonas knockouts using CRISPR/Cas9***

A CRISPR/Cas9-based targeted insertional mutagenesis approach[44] was used to knockout the *CrATG4 (Cre12.g510100*, Phytozome accession number, https://phytozome-next.jgi.doe.gov/. The same source was used for the *Chlamydomonas* genes below) and *CrATG5 (Cre14.g630907)* genes. For each gene, a guide RNA was designed for targeting the exon region in the 5' part of the gene of interest (**Table S1**). Electroporation was used to introduce a donor DNA comprising *Hsp70/RBCS2* promoter, *AphVIII* gene and *RBCS2* terminator, in addition to the ribonucleoprotein complex. The resulting transformants were screened with colony-PCR and confirmed by immunoblotting if specific antibodies were available.

***Transient expression in Arabidopsis protoplasts***

Protoplast were isolated from true leaves of 1.5-months-old plants of WT, *atg4a/b* and *atg7* backgrounds. Cells were then transformed with SH 17 and SH 19 constructs (**Table S2**) to overexpress mScarlet–ATG8F and mScarlet–ATG8I, respectively. Protoplast isolation, transformation and induction of autophagy was performed as previously described by Elander et al[45]. Cells were imaged using CLSM800 (Zeiss): 40x/1.2W lens, excitation light 561 nm and emission in the range of 570-650 nm.

Images were processed using ImageJ software[46] and a dedicated macro: https://github.com/AlyonaMinina/ImageJ-macros-for-CLSM-files-procesing.

***Genotyping of Arabidopsis lines***

Genomic DNA was extracted using a quick method. In brief, approximately 5 mg of plant material was lysed in 30 µl of 0.5 M NaOH by shaking together with glass beads, pH was then equilibrated with 370 µl of 0.1 M Tris-HCl, pH 6.8. Three µl of the resulting DNA solution was used for each PCR reaction.

*atg4a-2* mutation was verified using primer pairs annealing on the WT *ATG4A* allele (AM 409/AM 587, **Table S1**) and on the *atg4a-2* T-DNA insertion (AM 410/AM 584, **Table S1**). *atg4b-2* mutation was verified using primer pairs annealing on the wild-type *ATG4B* allele (AM 423/AM 420, **Table S1**) and on the *atg4b-2* T-DNA insertion (AM 420/AM 584, **Table S1**). Detection of the *atg5-1* T-DNA insertion was done using primers AM 1/AM 579 (**Table S1**), while wild-type ATG5 gene was detected with primers AM 1/AM 2 (**Table S1**).

***Isolation of the Chlamydomonas Genomic DNA***

Genomic DNA was isolated as previously described[47]. The cells were grown under standard conditions and harvested at a density of 1-2×$10^7$ cells $ml^{-1}$.

***RT-PCR***

Total RNA was extracted from 1.5-week-old Arabidopsis seedlings pooling 3 seedlings/extraction for each transgenic lines and using Spectrum™ Plant Total RNA Kit (Sigma-Aldrich, STRN250), RNAs were on-column treated with the DNase (Sigma-Aldrich, DNASE70-1SET) following the kit instructions. One µg of total RNA was used for each RT reaction implementing Maxima First Strand cDNA Synthesis Kit (ThermoFisher, K1641) and oligodT primers provided with the kit, and following the manufacturer's protocol. Full length cDNA of the ATG4A, ATG4B and WT were detected using primer pairs AM 417/AM 418, AM 419/AM 420, and AM 8/AM 9, respectively (Table S1). The amplicons were separated in a 1% TAE agarose gel containing GelRed dye and imaged with Chemi-Doc (Bio-Rad).

***In planta ATG8-CFP cleavage assay***

True leaves of one-month-old Arabidopsis plants expressing EosFP–ATG8A–CFP in *atg4a*, *atg4b, atg4a/b* and WT backgrounds were harvested and immediately flash-frozen in liquid nitrogen. Plant material was powdered while frozen and mixed 1:2 (m:V) with preheated 2xLaemmli buffer. Samples were boiled for 10 min at 95 °C and centrifugated at 17,000 *g* for 10 min. Seven and a half µl of each supernatant were loaded on a 4-20% TGX Stain-Free precast gel (Bio-Rad, 4568096). Separated proteins were transferred onto PVDF membrane (Bio-Rad) and blotted with anti-GFP (Roche, 11814460001) and anti-EosFP (Encorbio, RPCA-EosFP), both at 1:2,000 dilution. Anti-mouse (Amersham, NA931-1ML) and anti-rabbit (Invitrogen, a11008) HRP conjugates were used at 1:5,000 and 1:20,000 dilutions, respectively. Signal was developed using SuperSignal™ West Femto Maximum Sensitivity Substrate (ThermoFisher, 34094) and Chemi-Doc Imaging System (Bio-Rad).

***In vitro ATG8-CFP cleavage assay***

AM 810–813 plasmids (Table S2) encoding active and proteolytically dead (PD) GST-tagged AtATG4A and AtATG4B were used to transform Rosetta (DE3) cells (Novagen, 70954-3). Expression was induced overnight at 16°C using 0.25 mM IPTG (Hellobio, HB3941). Cell cultures were harvested by centrifugation at 5,000 *g* for 20 min, and the cell pellets were stored at –80°C until purification. Subsequent steps were conducted at 4°C. Cells were resuspended using a ratio of 1 g to 5 ml of binding buffer containing 20 mM PBS buffer, 100 mM NaCl, at pH 7.3. Lysis of the cells was achieved using a cell disruptor at 20,000 psi. The resulting sample was then treated with DNase I for 30 min. Insoluble cell debris was eliminated through centrifugation at 38,000 *g* for 20 min, followed by filtration of the supernatant through a 0.45 µm filter. The filtered supernatant was applied to an 8.5 mm diameter column packed with 1 ml of Glutathione Sepharose 4B matrix (Cytiva, 17075601) and equilibrated with the binding buffer. After sample application, the column was washed with approximately 10 column volumes of the binding buffer. The protein was eluted using an elution buffer containing 50 mM Tris-HCl, 100 mM NaCl, 10 mM reduced glutathione, at pH 8.0. Each fraction was collected after a 5-min incubation with the elution buffer. The protein

purity was assessed on 4–20% gradient SDS-PAGE gels. The purest fractions were combined and concentrated to 1 ml using Vivaspin 30K centrifugal concentrators (Sartorius, VS0621). The protein sample was then further purified by size exclusion chromatography on a HiLoad 16/600 Superdex 200 pg column (Cytiva, 28989335) connected to an ÄKTA FPLC system (Cytiva). The column was equilibrated with a buffer containing 50 mM Tris-HCl, 100 mM NaCl, 1 mM DTT at pH 8.0. Protein fractions were analysed with SDS-PAGE, pooled and concentrated to desired concentration. The protein concentration was calculated based on the measured A280 nm using a NanoDrop 1000 Spectrophotometer and the theoretical molar extinction coefficient determined using the ProtParam tool on the ExPASy server.[48] Before storing at –20°C protein sample was mixed with glycerol in a1:1 ratio.

True leaves of one-month-old Arabidopsis plants expressing EosFP–ATG8A-CFP in *atg4a/b* and WT backgrounds were harvested and immediately flash-frozen in liquid nitrogen. Plant material was powdered while frozen and mixed 1:2 (m:V) with reaction buffer containing 50 mM Tris pH 7.5, 100 mM NaCl, 5 mM DTT, 5 mM EDTA, 5 mM PMSF, 0.05% Tween-20 and 50 ng of purified active or PD ATG4. Reactions were kept at room temperature for the indicated period of time, prior to be mixed 1:1 with preheated 2xLaemmli buffer. Detection of EosFP and CFP in the reaction were preformed using Western blot assay as described for the *in planta* ATG8-CFP cleavage assay.

***Autophagy induction***

Induction of autophagy in Arabidopsis seedlings was performed in liquid 0.5xMS medium complemented with 5 µM AZD8055 (Santa-Cruz Biotech, 364424) and 0.5 µM concanamycin A (Santa-Cruz Biotech, 202111A). Treatment for 2 h was sufficient for induction of autophagy in seedlings roots, while treatment for 24 h was used for cotyledons.

For autophagy induction in older plants, the abaxial side of true leaves were infiltrated with MQ water containing 5 µM AZD and 0.5 µM ConA. The adaxial side of the infiltrated leaves was imaged after 24 h of treatment.

Treatments with 10 mM N-ethylmaleimide (NEM, Sigma-Aldrich 04259) and 1 mM iodoacetamide (IAM, Cytiva RPN6302) were performed simultaneously with AZD and ConA due to high phytotoxicity of the NEM and IAM. These treatments were performed using the approach described above for AZD/ConA. E64d showed lower toxicity in Arabidopsis, therefore plant material was pretreated with 5 µM E64d (Sigma-Aldrich E8640) prior to autophagy induction with AZD/ConA.

Nitrogen depleted conditions were implemented by growing the seedlings starting from seed germination on 0.5xMS devoid of nitrogen source: 0.5xMS basal salt mix (Sigma-Aldrich M0529): 1.5 mM $CaCl_2$, 0.75 mM $MgSO_4$, 0.25 mM $KH_2PO_4$, 2.5 mM KCl, 1% sucrose and 0.8% Plant agar.

Carbon depleted conditions were achieved by using 0.5xMS (described above) without sucrose and keeping plants in the dark.

***Confocal microscopy***

Confocal microscopy was preformed using CSLM SP8 (Leica) and CLSM 800 (Zeiss), in either case using 40x water immersion lens, NA=10–1.2. GFP, CFP and EosFP were imaged using excitation light of 488 nm and emission range 515–560 nm. Red fluorescence was detected using 561 nm excitation light and 570–650 nm emission.

To prevent root desiccation during imaging, seedlings were mounted inside RoPod chambers[49], in a droplet of liquid corresponding to the treatment. Detached cotyledons were imaged while mounted between two coverslips. Sections of true leaves were mounted in a droplet of liquid between standard microscopy slide and a coverslip additionally secured with tape. True leaves and cotyledons were imaged only from the adaxial side.

Confocal images were processed using LAS X (for Leica micrographs) software or ImageJ[46] implementing the dedicated macro for channel separation and image cropping: https://github.com/AlyonaMinina/ImageJ-macros-for-CLSM-files-procesing.

***Quantification of autophagic bodies density and area***

Quantification of autophagic bodies was performed in a semi-automated manner using ImageJ software and custom-made macro. The puncta quantification shown in Fig. 2 was done using the macro for puncta quantification in

single channel v4. It can be found in the dedicated GitHub repository: https://github.com/AlyonaMinina/Puncta-quantification-with-ImageJ.

The quantifications shown in Figs. 4 and S3 were obtained using macro for autophagic body size and density measurement: https://github.com/AlyonaMinina/Autophagic-bodies-size-measurement.

Each experiment was performed at least twice, using at least three biological replicates (individual plants) and three technical replicates (images of representative areas on the same plant). Unless stated otherwise, results were subjected to Tukey's HSD test. Plots were built using the ggplot2 R package[50].

***Western blotting***

Whole Arabidopsis seedlings or a section of true leaf were sampled into liquid nitrogen and powdered while frozen. A pool of 4–8 seedlings per sample or sections from three different leaves were used as one sample to ensure representativity of the data. To limit potential protein proteolysis during sample preparation, the powdered material was directly mixed with preheated Laemmli buffer in 1:2 (m:V) ratio. Samples were boiled at 95°C for 10 min, mixing every 2 min. Debris was removed by centrifugation at 17,000 *g* for 10 min. Supernatants were transferred into new Eppendorf tubes and stored at –20°C. Typically, 7.5-15 µl of each sample were used for separation on the gel.

To separate tagged ATG8 and tagged ATG8–PE adducts, 10% PAAG was prepared manually supplementing it with 6 M urea[35,51]. To ensure sufficient separation of the tagged ATG8 adducts, the electrophoresis was performed until the 25 kDa band of the prestained PageRuler (ThermoFisher Scientific, 26619) reached the bottom edge of the gel. For other Western blot assays, proteins were separated on 4–20% TGX Stain-Free precast gels (Bio-Rad, 4568096). Detections of the EosFP, GFP and CFP was performed using Western blot assay as described for the *in planta* ATG8–CFP cleavage assay.

Total proteins from *Chlamydomonas* cells were extracted as described in Zou et al., (2023)[47]. The cells were grown under standard conditions and harvested at a density of 1-2×$10^7$ cells $ml^{-1}$. The antibodies of CrATG4 were purchased from Agrisera (AS15 2831) and used at dilution 1:5,000 for western blot. Anti-rabbit HRP-conjugate from Agrisera (AS07 260) was used at a dilution of 1:10,000.

***Plant phenotyping***

Root growth assays were performed using SPIRO[25] for automated imaging of Petri plates and SPIRO assays for image analysis. To ensure reproducibility of the conditions and therefore comparability of the results, SPIRO robots were placed inside the same plant growth cabinets that were used for growing seedling on plates in other experiments of this study. For experiments illustrated in Fig. 3, Movies S2 and S3, seeds were plated directly on the corresponding medium used for the stress induction and plates were imaged without interruption during day and night for at least seven days, utilizing green LED of SPIRO for imaging in the dark. For carbon starvation assays, seedlings were allowed to grow under long day conditions for 4–5 days, followed by 4 days of dark treatment and another 4 days of recovery.

For the experiments shown in Fig. 4I and 4J seeds of the T2 generation, showing red fluorescent signal of the FastRed marker, were first germinated on standard 0.5xMS medium. Roots of 4-days-old seedlings were checked with a stereoscope to ensure strong and even GFP signal. Seedlings with confirmed transgene expression were then transferred onto –N medium and imaged using SPIRO for 7 days.

SPIRO data analysis was performed as described by Ohlsson et al [25].

Photos of plants in soil were obtained using the camera of an iPhone XI and further processed in Photoshop 25.0.0.

***Senescence assay in Chlamydomonas***

The *Chlamydomonas* cells were pre-cultured until they reached the early stationary phase. The cells were then subjected to ten times dilution using fresh TAP medium. Upon attaining the late log phase or stationary phase, 1x$10^5$ cells were inoculated on TAP agar plates for senescence assay. Cell colonies were imaged after 40 days.

***Protein alignment and tree building***

Protein sequence alignments and construction of the phylogenetic tree was done in the Geneious software v10.2.6.

## References


1. Mizushima, N. A brief history of autophagy from cell biology to physiology and disease. *Nat Cell Biol* **20**, 521–527 (2018).
2. Kraft, C. & Reggiori, F. Phagophore closure, autophagosome maturation and autophagosome fusion during macroautophagy in the yeast Saccharomyces cerevisiae. *FEBS Lett* (2023) doi:10.1002/1873-3468.14720.
3. Marshall, R. S. & Vierstra, R. D. Autophagy: The Master of Bulk and Selective Recycling. *Annu Rev Plant Biol* **69**, 173–208 (2018).
4. Ichimura, Y. *et al.* A ubiquitin-like system mediates protein lipidation. *Nature* **408**, 488–492 (2000).
5. Romanov, J. *et al.* Mechanism and functions of membrane binding by the Atg5-Atg12/Atg16 complex during autophagosome formation. *EMBO Journal* **31**, (2012).
6. Martens, S. & Fracchiolla, D. Activation and targeting of ATG8 protein lipidation. *Cell Discov* **6**, 23 (2020).
7. Kirisako, T. *et al.* The reversible modification regulates the membrane-binding state of Apg8/Aut7 essential for autophagy and the cytoplasm to vacuole targeting pathway. *Journal of Cell Biology* **151**, 263–275 (2000).
8. Abreu, S. *et al.* Conserved Atg8 recognition sites mediate Atg4 association with autophagosomal membranes and Atg8 deconjugation. *EMBO Rep* e201643146–e201643146 (2017) doi:10.15252/embr.201643146.
9. Yoshimoto, K. Processing of ATG8s, Ubiquitin-Like Proteins, and Their Deconjugation by ATG4s Are Essential for Plant Autophagy. *the Plant Cell Online* **16**, 2967–2983 (2004).
10. Nair, U. *et al.* A role for Atg8-PE deconjugation in autophagosome biogenesis. *Autophagy* **8**, (2012).
11. Nakatogawa, H., Ishii, J., Asai, E. & Ohsumi, Y. Atg4 recycles inappropriately lipidated Atg8 to promote autophagosome biogenesis. *Autophagy* **8**, 177–186 (2012).
12. Kauffman, K. J. *et al.* Delipidation of mammalian Atg8-family proteins by each of the four ATG4 proteases. *Autophagy* **14**, 1–19 (2018).
13. Yu, Z.-Q. *et al.* Dual roles of Atg8-PE deconjugation by Atg4 in autophagy. *Autophagy* **8**, 883–892 (2012).
14. Kellner, R. *et al.* ATG8 Expansion : A Driver of Selective Autophagy Diversi fi cation ? *Trends Plant Sci* **22**, 204–214 (2017).
15. Rodriguez-Furlan, C. *et al.* Interaction between VPS35 and RABG3f is necessary as a checkpoint to control fusion of late compartments with the vacuole. *Proceedings of the National Academy of Sciences* **116**, 21291–21301 (2019).
16. Yao, S., Peng, S. & Wang, X. Phospholipase Dε interacts with autophagy-related protein 8 and promotes autophagy in Arabidopsis response to nitrogen deficiency. *The Plant Journal* **109**, 1519–1534 (2022).
17. Dauphinee, A. N. *et al.* Chemical screening pipeline for identification of specific plant autophagy modulators. *Plant Physiol* **181**, 855–866 (2019).
18. Thompson, A. R. Autophagic Nutrient Recycling in Arabidopsis Directed by the ATG8 and ATG12 Conjugation Pathways. *Plant Physiol* **138**, 2097–2110 (2005).
19. Esther Pérez-Pérez, M., Zaffagnini, M., Marchand, C. H., Crespo, J. L. & Lemaire, S. D. The yeast autophagy protease Atg4 is regulated by thioredoxin View supplementary material. (2014) doi:10.4161/auto.34396.
20. Agrotis, A., Pengo, N., Burden, J. J. & Ketteler, R. Redundancy of human ATG4 protease isoforms in autophagy and LC3/GABARAP processing revealed in cells. (2019) doi:10.1080/15548627.2019.1569925.
21. Maruyama, T. & Noda, N. N. Autophagy-regulating protease Atg4: structure, function, regulation and inhibition Tatsuro Maruyama and Nobuo N Noda. (2018) doi:10.1038/ja.2017.104.
22. Klionsky, D. J. *et al.* Guidelines for the use and interpretation of assays for monitoring autophagy (3rd edition). *Autophagy* vol. 12 1554-8635 (Online) Preprint at https://doi.org/10.1080/15548627.2015.1100356 (2016).
23. Abreu, S. *et al.* Conserved Atg8 recognition sites mediate Atg4 association with autophagosomal membranes and Atg8 deconjugation. *EMBO Rep* e201643146 (2017) doi:10.15252/embr.201643146.

24. Chung, T., Phillips, A. R. & Vierstra, R. D. ATG8 lipidation and ATG8-mediated autophagy in Arabidopsis require ATG12 expressed from the differentially controlled ATG12A and ATG12B loci. *Plant Journal* **62**, 483–493 (2010).

25. Ohlsson, J. A. *et al.* SPIRO-the automated Petri plate imaging platform designed by biologists, for biologists. *bioRxiv* (2023) doi:https://doi.org/10.1101/2021.03.15.435343.

26. Waadt, R. *et al.* Dual-Reporting Transcriptionally Linked Genetically Encoded Fluorescent Indicators Resolve the Spatiotemporal Coordination of Cytosolic Abscisic Acid and Second Messenger Dynamics in Arabidopsis. doi:10.1105/tpc.19.00892.

27. Yoshimoto, K. *et al.* Autophagy Negatively Regulates Cell Death by Controlling NPR1-Dependent Salicylic Acid Signaling during Senescence and the Innate Immune Response in Arabidopsis. *THE PLANT CELL ONLINE* **21**, 2914–2927 (2009).

28. Kajikawa, M. *et al.* Isolation and Characterization of Chlamydomonas Autophagy-Related Mutants in Nutrient-Deficient Conditions. doi:10.1093/pcp/pcy193.

29. Koumandou, V. L. *et al.* Molecular paleontology and complexity in the last eukaryotic common ancestor. *Crit Rev Biochem Mol Biol* **48**, 373–396 (2013).

30. Chen, Y. & Yu, L. Development of Research into Autophagic Lysosome Reformation. *Mol Cells* **41**, 45–49 (2018).

31. Yim, W. W. Y. & Mizushima, N. Lysosome biology in autophagy. *Cell Discov* **6**, (2020).

32. Suttangkakul, A., Li, F., Chung, T. & Vierstra, R. D. The ATG1/ATG13 protein kinase complex is both a regulator and a target of autophagic recycling in Arabidopsis. *Plant Cell* **23**, 3761–3779 (2011).

33. Feng, Y., He, D., Yao, Z. & Klionsky, D. J. The machinery of macroautophagy. *Cell Res* **24**, 24–41 (2014).

34. Zess, E. K. *et al.* N-terminal β-strand underpins biochemical specialization of an ATG8 isoform. *PLoS Biol* **17**, (2019).

35. Chung, T., Phillips, A. R. & Vierstra, R. D. ATG8 lipidation and ATG8-mediated autophagy in Arabidopsis require ATG12 expressed from the differentially controlled ATG12A and ATG12B loci. *Plant Journal* **62**, 483–493 (2010).

36. Hofius, D. *et al.* Autophagic Components Contribute to Hypersensitive Cell Death in Arabidopsis. *Cell* **137**, 773–783 (2009).

37. Neupert, J., Karcher, D. & Bock, R. Generation of Chlamydomonas strains that efficiently express nuclear transgenes. doi:10.1111/j.1365-313X.2008.03746.x.

38. Lampropoulos, A. *et al.* GreenGate - A novel, versatile, and efficient cloning system for plant transgenesis. *PLoS One* **8**, (2013).

39. Grefen, C. *et al.* A ubiquitin-10 promoter-based vector set for fluorescent protein tagging facilitates temporal stability and native protein distribution in transient and stable expression studies. *Plant Journal* **64**, (2010).

40. Nakagawa, T. *et al.* Improved gateway binary vectors: High-performance vectors for creation of fusion constructs in transgenic analysis of plants. *Biosci Biotechnol Biochem* **71**, (2007).

41. Crozet, P. *et al.* Birth of a Photosynthetic Chassis: A MoClo Toolkit Enabling Synthetic Biology in the Microalga Chlamydomonas reinhardtii. (2018) doi:10.1021/acssynbio.8b00251.

42. Neupert, J., Shao, N., Lu, Y. & Bock, R. Genetic transformation of the model green alga Chlamydomonas reinhardtii. *Methods in Molecular Biology* **847**, (2012).

43. Clough, S. J. & Bent, A. F. Floral dip: A simplified method for Agrobacterium-mediated transformation of Arabidopsis thaliana. *Plant Journal* **16**, 735–743 (1998).

44. Picariello, T. *et al.* TIM, a targeted insertional mutagenesis method utilizing CRISPR/Cas9 in Chlamydomonas reinhardtii. (2020) doi:10.1371/journal.pone.0232594.

45. Elander, P. H. *et al.* Interactome of Arabidopsis ATG5 Suggests Functions beyond Autophagy. *Int J Mol Sci* **24**, 12300 (2023).

46. Schindelin, J. *et al.* Fiji: An open-source platform for biological-image analysis. *Nat Methods* **9**, 676–682 (2012).

47. Zou, Y. *et al.* Thermoprotection by a cell membrane-localized metacaspase in a green alga 1 2. doi:10.1101/2023.04.28.538660.

48. Gasteiger, E. *et al.* Protein Identification and Analysis Tools on the ExPASy Server; The Proteomics Protocols Handbook. *Humana Press* **112**, (2005).

49. Guichard, M., Holla, S., Wernerová, D., Grossmann, G. & Minina, E. A. RoPod , a customizable toolkit for non-invasive root imaging , reveals cell type-specific dynamics of plant autophagy. 1–21 (2021).

50. Ginestet, C. ggplot2: Elegant Graphics for Data Analysis. *J R Stat Soc Ser A Stat Soc* **174**, (2011).

51. Minina, E. A. *et al.* Transcriptional stimulation of rate-limiting components of the autophagic pathway improves plant fitness. *J Exp Bot* **69**, 1415–1432 (2018).

## Supplementary material

| | |
|---|---|
| **Figure S1** | Expression of ATG8E □C restores accumulation of puncta in the vacuoles of ATG4-deficeint Arabidopsis roots. |
| **Figure S2** | Verification of the transgenic lines used in the study. |
| **Figure S3** | Detection of autophagic bodies in true leaves of plants expressing ATG8E □C. |
| **Figure S4** | Efficient delipidation of ATG8E □C in Arabidopsis requires expression of both ATG4 proteases. |
| **Figure S5** | Expression of ATG8E ΔC complements autophagy-deficient shoot phenotypes of *atg4a/b*. |
| **Figure S6** | Transient overexpression of the naturally truncated ATG8I isoform restores accumulation of autophagic bodies in the vacuoles of *atg4a/b* cells. |
| **Figure S7** | Overexpression of the naturally truncated ATG8I isoform in the WT leads to a decreased autophagic activity efficiency under nitrogen-depleted conditions. |
| **Figure S8** | Validation of generated *Chlamydomonas ATG4* and *ATG5* knockout mutants. |
| **Movie S1** | Chemical inhibition of ATG4 activity with IAM and NEM does not prevent accumulation of autophagic bodies in true leaves. |
| **Movie S2** | ATG8E ΔC complements stunted root growth phenotype of *atg4a/b* under nitrogen-depleted conditions. |
| **Movie S3** | ATG8E ΔC complements weak root growth recovery of *atg4a/b* after carbon-depletion. |
| **Table S1** | Primers used in this study |
| **Table S2** | Plasmids used in this study |
| **Table S3** | Arabidopsis transgenic lines used in this study |

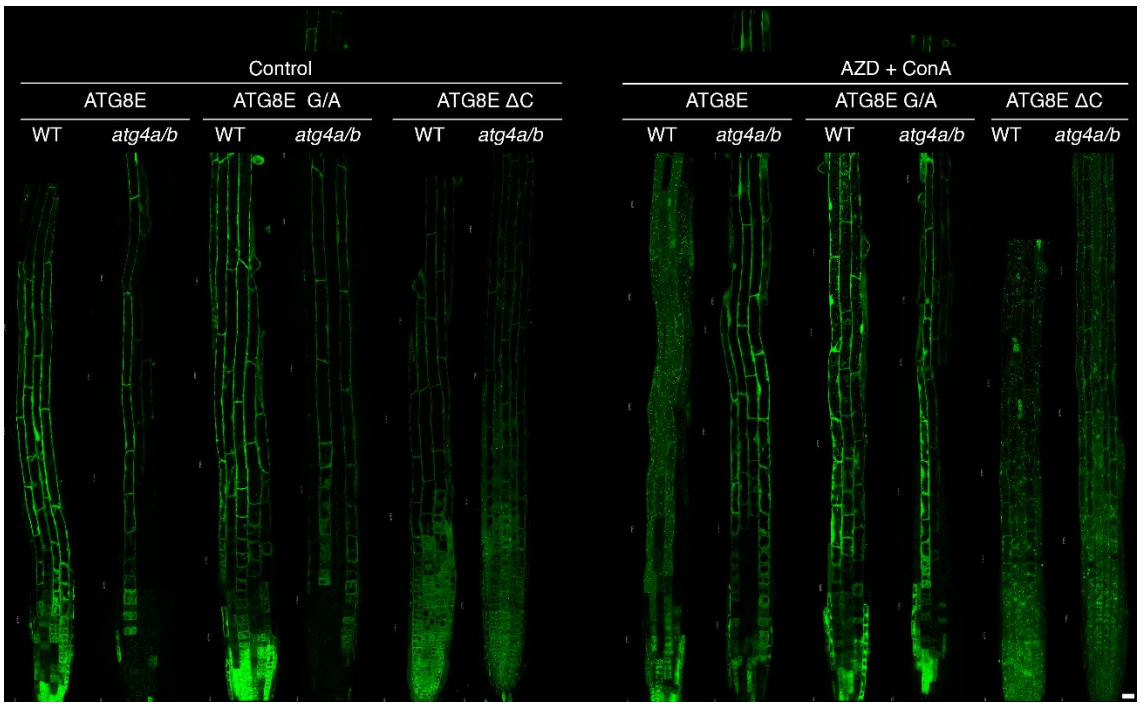


**Figure S1**. **Expression of ATG8E ΔC restores accumulation of puncta in the vacuoles of ATG4-deficeint Arabidopsis roots.**

Complete tile-scans of roots partially shown in **Fig. 1 D**. Control, roots incubated and imaged in the standard 0.5xMS growth medium; AZD + ConA, roots incubated and imaged in the 0.5xMS medium supplemented with 5 µM AZD8055 and 0.5 µM concanamycin A. Scale bar, 20 µm.

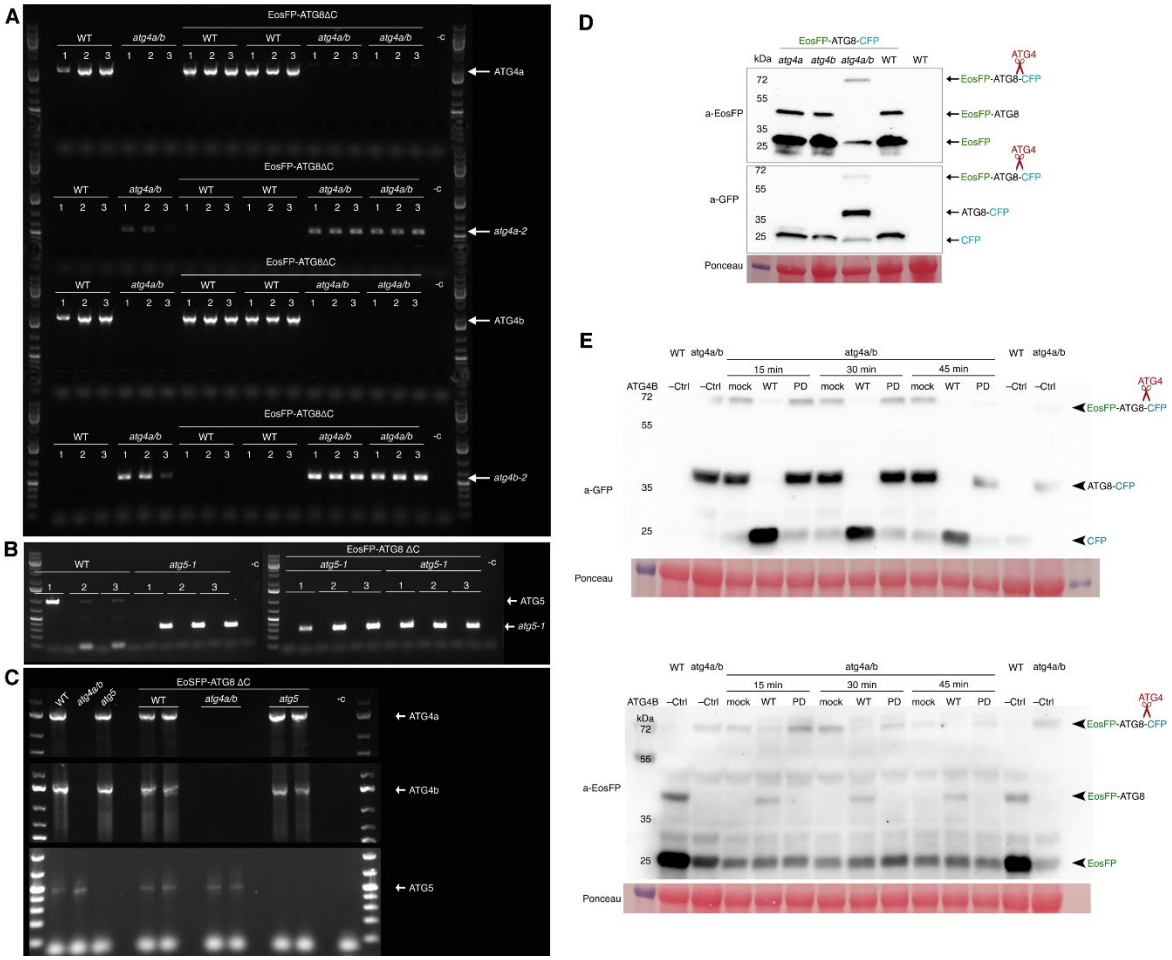


**Figure S2. Verification of the transgenic lines used in the study.**

**A**. Genotyping of Arabidopsis lines to detect WT *ATG4A* and *ATG4B* alleles as well as *atg4a-2* and *atg4b-2* T-DNA insertions. The results confirm absence of complete *ATG4* genes in all lines with *atg4a/b* background.

**B**. Genotyping of Arabidopsis lines to detect WT *ATG5* allele as well as *atg5-1* T-DNA insertion.

**C**. RT-PCR confirms absence of full length *ATG4* mRNAs in the *atg4a/b* lines. Similarly, *atg5-1* lines do not contain full length *ATG5* transcript.

**D**. Lack of ATG4 proteolytic activity in the *atg4a/b* double knockout was confirmed by Western blot detection of the EosFP–ATG8–CFP fusion protein in the total protein extracts of plants stably expressing the fusion in the WT, *atg4a*, *atg4b,* and *atg4a/b* backgrounds. The product of cleavage by ATG4, EosFP–ATG8, was not detectable in the *atg4a/b* knockout line. Notably expression of either of the ATG4 proteases is sufficient to process all the ectopically overexpressed EosFP–ATG8–CFP fusion protein.

**E**. Processing of the EosFP–ATG8–CFP fusion by ATG4 protease was corroborated in the *in vitro* assay. Total protein extracts of plants stably expressing EosFP–ATG8-CFP fusion in *atg4a/b* background was incubated together with a buffer (mock), recombinant active ATG4B (WT) or its proteolytically dead mutant (PD) for 15, 30, or 45 min. The reactions were loaded on the polyacrylamide gel and subjected to Western blotting detecting EosFP tag. Additionally, total protein extracts of plants expressing the same fusion protein in the WT and ATG4-deficient background were mixed directly with loading buffer and used as additional controls for fusion protein stability *in vivo* (WT –Ctrl and *atg4a/b* –Ctrl, respectively). Cleavage of the bond between ATG8 and CFP was observed only in the presence of active ATG4.

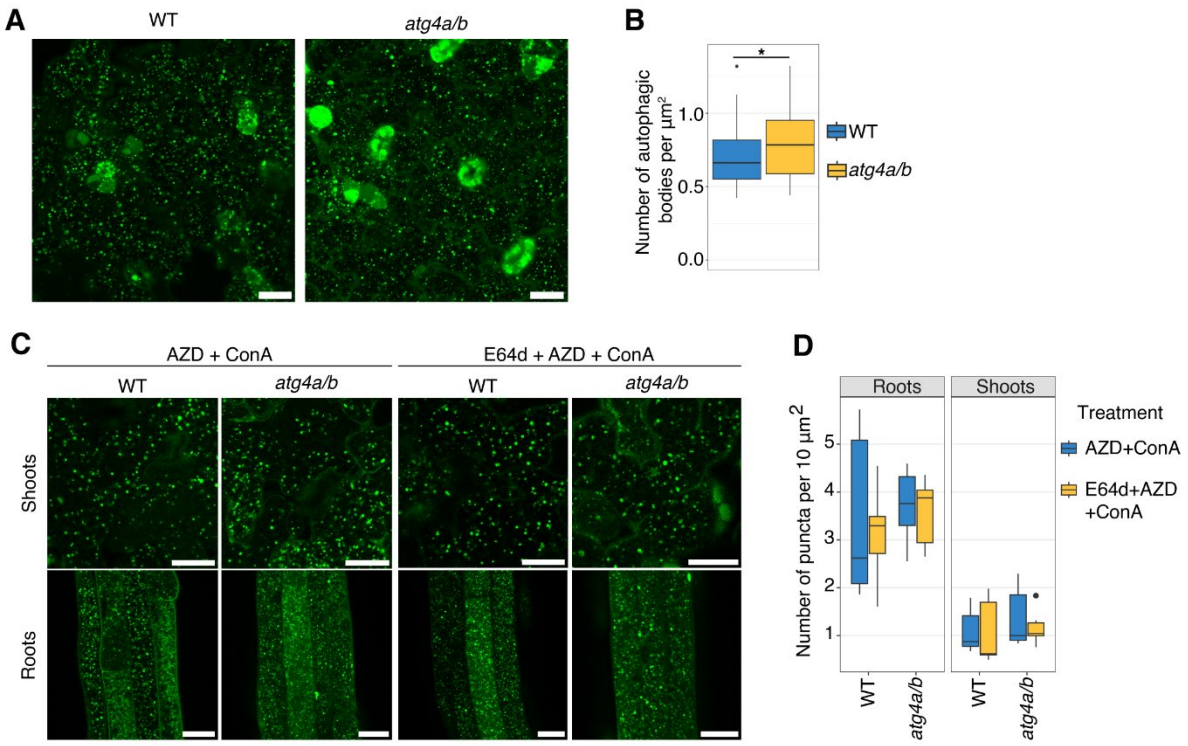


**Figure S3. Detection of autophagic bodies in true leaves of plants expressing ATG8E ΔC.**

**A**. Confocal microscopy images of leaf epidermal cells of 1.5-months-old Arabidopsis plants expressing EosFP–ATG8E ΔC in WT or ATG4-deficient backgrounds. Leaves were infiltrated with AZD/ConA solution 24 h prior to imaging. Scale bars, 20 µm.

**B.** Quantification of puncta per vacuolar area for the samples illustrated in **A**. The chart shows representative results of one out of two experiments, $n = 90$. The samples differ according to Welch's *t*-test, *, $p < 0.05$. Boxes indicate interquartile region (IQR); median is indicated by a horizontal line; whiskers represent range within 1.5 IQR; outliers are represented by solid a filled circle.

**C.** Confocal microscopy images of root and shoot epidermal cells of 7-days-old Arabidopsis seedlings expressing EosFP–ATG8E ΔC in WT or *ATG4* knockout. Seedlings were treated for 8 h with the cysteine protease inhibitor E64d prior to induction of autophagy with AZD/ConA. Scale bars, 20 µm.

**D.** Quantification of puncta per vacuolar area on the data illustrated in **C**. Tukey's HSD test was performed for each plant organ individually, no statistically significant difference was discovered at the $\alpha = 0.05$ level; $n = 36$ for each organ. Boxes indicate interquartile region (IQR); median is indicated by a horizontal line; whiskers represent range within 1.5 IQR; outliers are represented by a filled circle. The chart shows representative results for one out of two experiments.

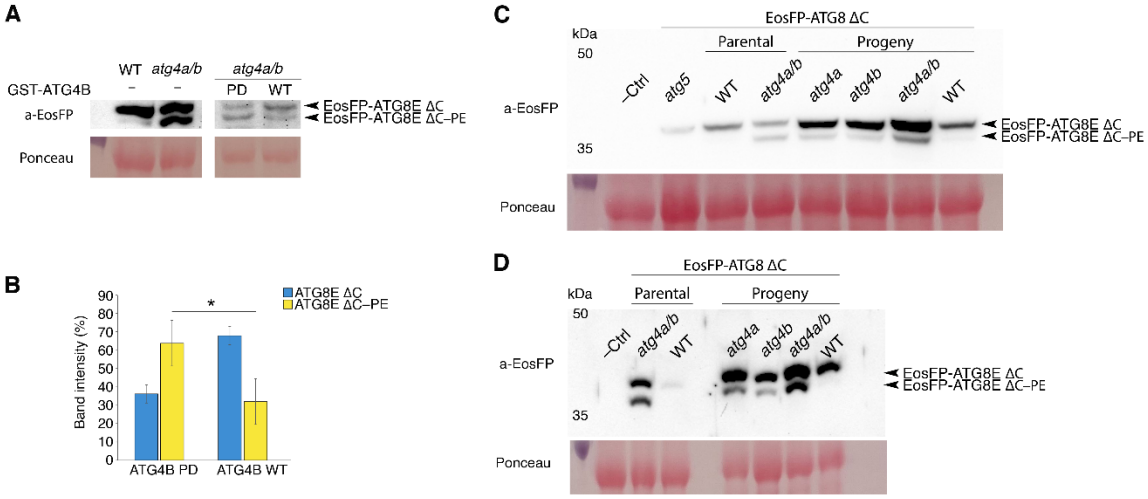


**Figure S4. Efficient delipidation of ATG8E ΔC in Arabidopsis requires expression of both ATG4 proteases.**

**A**. *In vitro* ATG8 delipidation assay. Left panels: higher accumulation of the ATG8–PE adduct in *atg4a/b* plants expressing EosFP-ATG8E ΔC compared to WT was confirmed by immunodetection of EosFP in total protein extracts obtained by mixing plant material with hot Laemmli buffer. Right panels: total protein extract of *atg4a/b* plant expressing EosFP-ATG8E ΔC was incubated with recombinant active GST-ATG4B (WT) or its proteolytically dead mutant (PD) prior to Western blot detection of the EosFP tag. Ponceau S staining was used as a loading control.

**B**. Quantification of the EosFP–ATG8E ΔC and EosFP– ATG8E ΔC–PE bands intensity illustrated in **A** shows significant decrease in the ATG8–PE content in the presence of active ATG4B. Band intensity is expressed as a percentage of the sum intensity for both bands in each sample. Error bars indicate StDev. Chart shows results for two independent experiments. Student's t-test at the $\alpha = 0.05$ level; *, $p < 0.001$, $n = 24$.

**C**. Western blot detection of EosFP tag in the total protein extract of 14-days-old Arabidopsis seedlings expressing EosFP–ATG8E ΔC in the WT, ATG5-, ATG4A-, ATG4B-, and ATG4A/B-deficient backgrounds. Sampling was done without any prior treatment. –Ctrl, negative control (extract of Arabidopsis seedlings not expressing EosFP tagged proteins). Ponceau S staining was used as a loading control. Single *ATG4*-knockout plants were obtained by crossing *atg4a/b* plants with WT. Parental, plants grown from seed used for crossing; progeny, plants grown from F2 generation seeds obtained from the crosses. Seedlings were genotyped prior to protein extraction to confirm the genetic background.

**D**. Detection of the EosFP–ATG8–PE form in the total protein extracts from 1.5-months-old plants corroborates observations made on seedlings and illustrated in **A**: both ATG4 proteases are required for efficient delipidation of ATG8E ΔC. Sampling was done without any prior treatment.

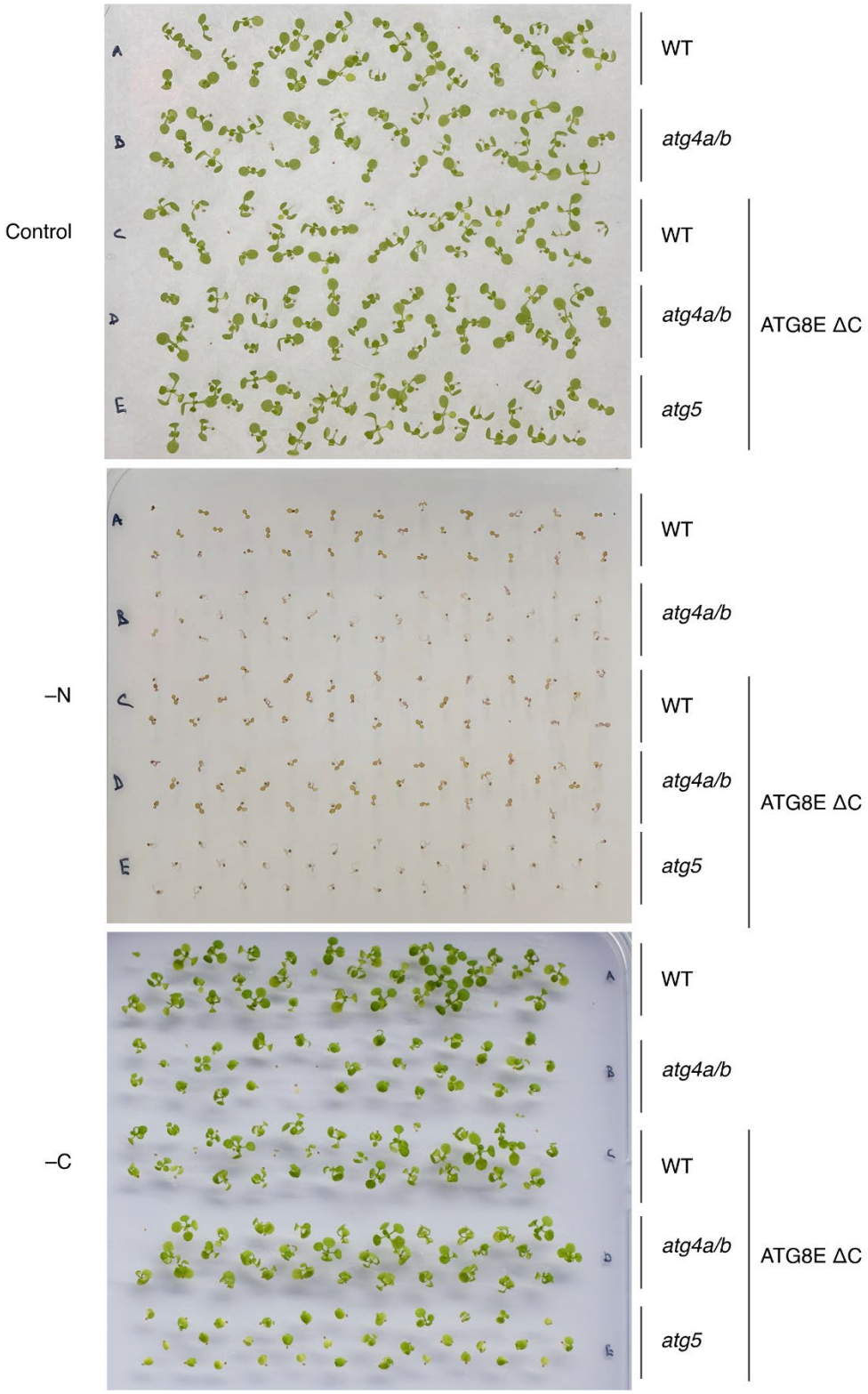


**Figure S5. Expression of ATG8E ΔC complements autophagy-deficient shoot phenotypes of *atg4a/b*.**
Images of Petri plates with Arabidopsis seedlings grown on 0.5x MS medium (Control), nitrogen-depleted (–N) medium or carbon-depleted (–C) medium. Autophagy-deficient seedlings have decreased viability under –N conditions (quantification shown **Fig. 3E**). However, *atg4a/b* seedling expressing ATG8E ΔC exhibit wild-type-like viability. Seedlings grown on –C medium were subjected to seven days of dark treatment followed by seven days of recovery prior to imaging. Autophagy-deficient seedlings are slower to recover compared to both wild-type seedlings and *atg4a/b* seedlings expressing ATG8E ΔC (quantification shown **Fig. 3F**).

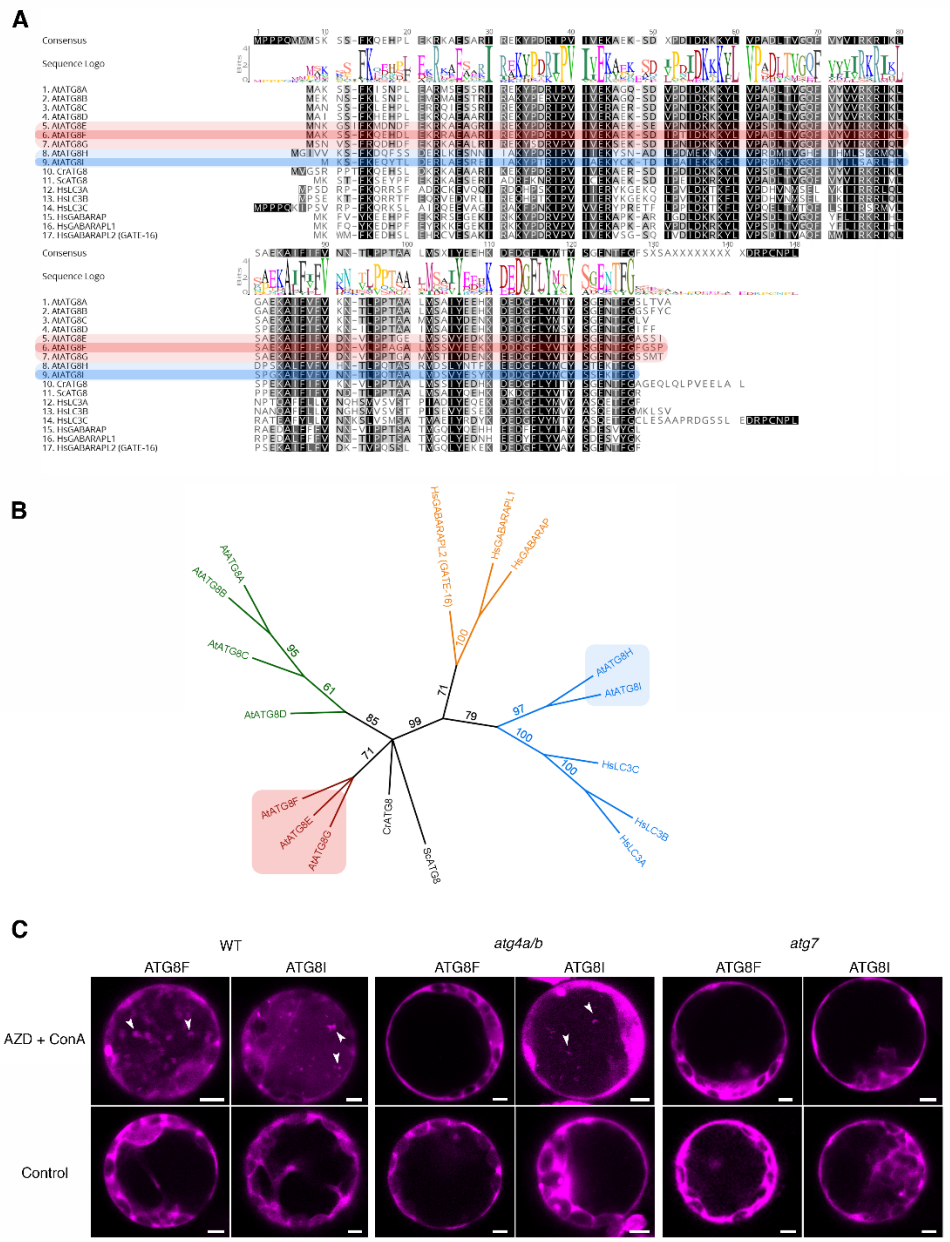


**Figure S6. Transient overexpression of the naturally truncated ATG8I isoform restores accumulation of autophagic bodies in the vacuoles of *atg4a/b* cells.**

**A**. Clustal W protein sequence alignment of *Arabidopsis thaliana* (At), *Chlamydomonas reinhardtii* (Cr), *Saccharomyces cerevisiae* (Sc) and *Homo sapiens* (Hs) orthologs of ATG8. Red and blue rectangles highlight Arabidopsis orthologs most similar to the highest express full-length and truncated versions of ATG8. Darker colour rectangles highlight sequences of the highest expressed Arabidopsis ATG8 orthologs: ATG8F and ATG8I.

**B**. Phylogenetic tree illustrating evolutionary distances of ATG8 proteins compared in **A**, shows the separation of Arabidopsis ATG8s into the previously described two clades (Kellner et al., 2017): Clade I, more similar to fungi and comprising only complete ATG8s containing the C-terminus, and Clade II, comprising natively truncated ATG8s, more similar to animal ATG8s.

**C**. mScarlet–ATG8F or mScarlet–ATG8I were transiently expressed in mesophyll protoplasts of WT, *atg4a/b,* or *atg7* Arabidopsis plants. An aliquot of each transformed protoplast suspension was subjected to AZD/ConA treatment for 17 h prior to imaging. Scale bar = 5 µm. White arrow heads indicate autophagic bodies.

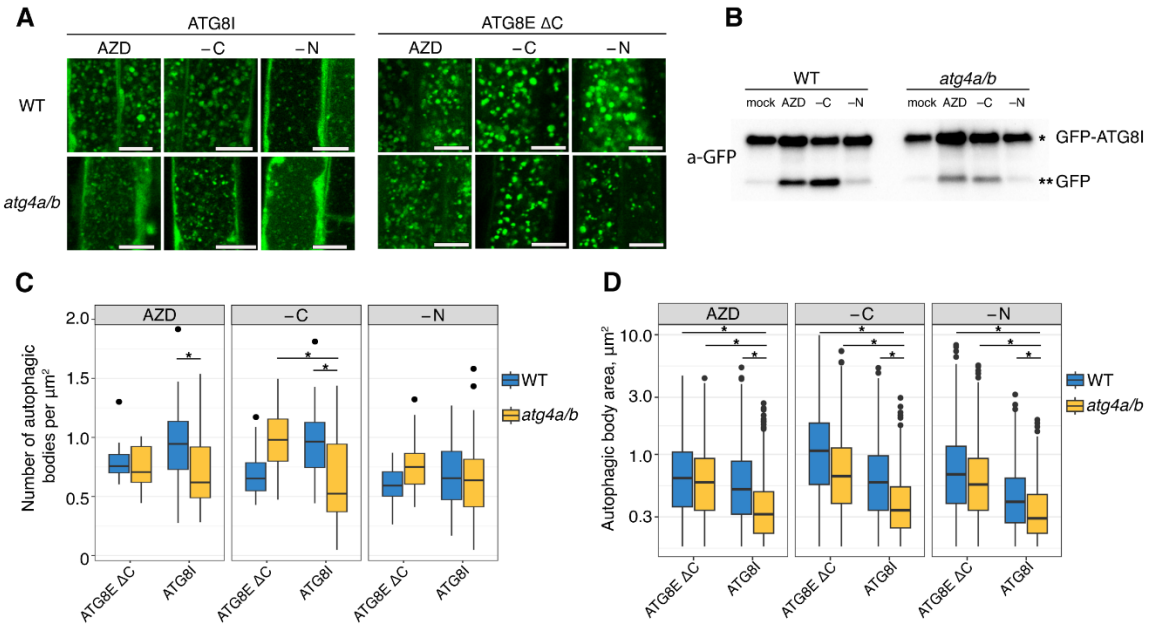


**Figure S7. Overexpression of the naturally truncated ATG8I isoform in the WT leads to a decreased autophagic activity efficiency under nitrogen-depleted conditions.**

**A.** Confocal microscopy images showing phenotypes of autophagic bodies in the vacuoles of root epidermal cells of seedlings expressing ATG8E ΔC or ATG8I in WT and *atg4a/b* backgrounds. Seven days old Arabidopsis seedlings were subjected to treatments for 24 h prior to imaging. The treatments included AZD/ConA, –C/ConA , and –N/ConA. Scale bars, 10 µm.

**B.** GFP cleavage assay performed on the seedlings illustrated in **A** confirms autophagic activity under all three stress conditions used in the experiment.

**C**. Quantification of autophagic bodies for the data illustrated in **A** confirms autophagic activity under all three conditions used in the experiment. Boxes indicate interquartile region (IQR); median is indicated by a horizontal line; whiskers represent range within 1.5 IQR; outliers are represented by solid a filled circle. Dunnett's test vs *atg4a/b* expressing ATG8I was performed for each treatment. *, $p < 0.0001$. Dots indicate outliers.

**D**. Quantification of puncta areas in the samples illustrated in **A** reveals significant decrease of autophagic body size under nitrogen depleted conditions if ATG8I is overexpressed either in the WT or *atg4a/b* backgrounds. Boxes indicate interquartile region (IQR); median is indicated by a horizontal line; whiskers represent range within 1.5 IQR; outliers are represented by solid a filled circle. Dunnett's test vs *atg4a/b* expressing ATG8I was performed for each treatment. *, $p < 0.0001$. Dots indicate outliers.

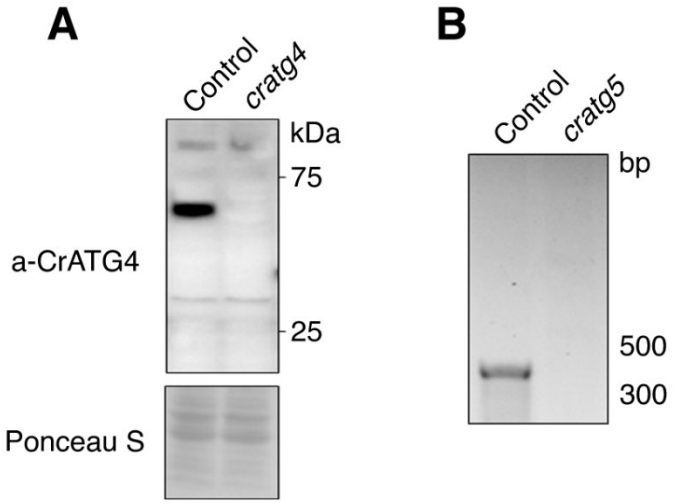


**Figure S8. Validation of generated *Chlamydomonas ATG4* and *ATG5* knockout mutants.**
**A**. Western blot detection of ATG4 protein in the total protein extracts of WT (Control) and *ATG4* knockout (*cratg4*) *Chlamydomonas* cells confirms absence of ATG4 protein in the knockout background. Ponceau S staining was used as a loading control.
**B**. Genotyping of the *ATG5* knockout mutant confirms deletion of the *ATG5* gene.

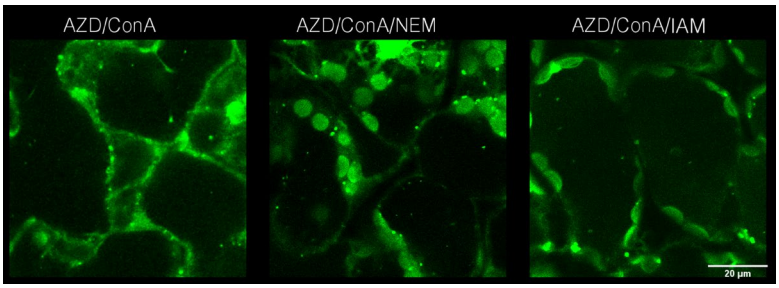


**Movie S1. Chemical inhibition of ATG4 activity with IAM and NEM does not prevent accumulation of autophagic bodies in true leaves.**

Representative time-lapse scans of mesophyll cells of Arabidopsis true leaves expressing EosFP–ATG8E ΔC in the WT background. Leaves of 1 month old plants were infiltrated with MQ water containing 5 µM AZD8055 and 0.5 µM ConA additionally supplemented with 1mM IAM (Iodoacetamide) or 10 mM NEM (N-ethylmaleimide) without detaching them from plants. Leaves were imaged using CLSM 24 h after the treatment start.

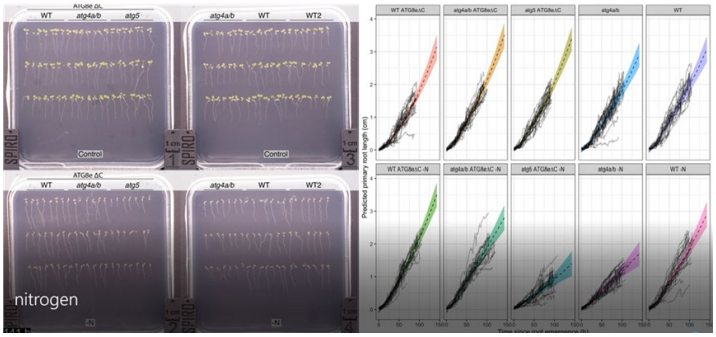


**Movie S2. ATG8E ΔC complements stunted root growth phenotype of *atg4a/b* under nitrogen-depleted conditions.**

Representative SPIRO time-lapse data showing seedlings on control medium (top two plates) and–N medium (bottom two plates) imaged simultaneously. Charts on the right show data from the SPIRO root growth tracking assay plotted for each seedling and combined by genotype/growth conditions. Autophagy-deficient genotypes (*atg4a/b* and *atg5* ATG8E ΔC) show stunted growth under –N conditions, while *atg4a/b* ATG8E ΔC seedlings have normal root elongation under the same conditions.

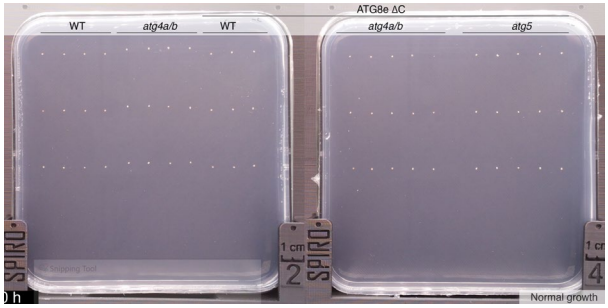


**Movie S3. ATG8E ΔC complements weak root growth recovery of *atg4a/b* after carbon-depletion.**

Representative SPIRO time-lapse data showing seedlings on carbon-depleted plates imaged simultaneously. Seeds were allowed to germinate and seedlings were grown under normal growth conditions, after which the lights in the growth cabinet were turned off and imaging proceeded for four days in the dark (carbon depletion), followed by imaging for another four days under normal growth conditions (recovery).

Roots of autophagy-deficient seedlings (*atg4a/b* and *atg5* ATG8E ΔC) do not restart growth during recovery stage, while roots of *atg4a/b* ATG8E ΔC seedlings elongate normally under the same conditions.

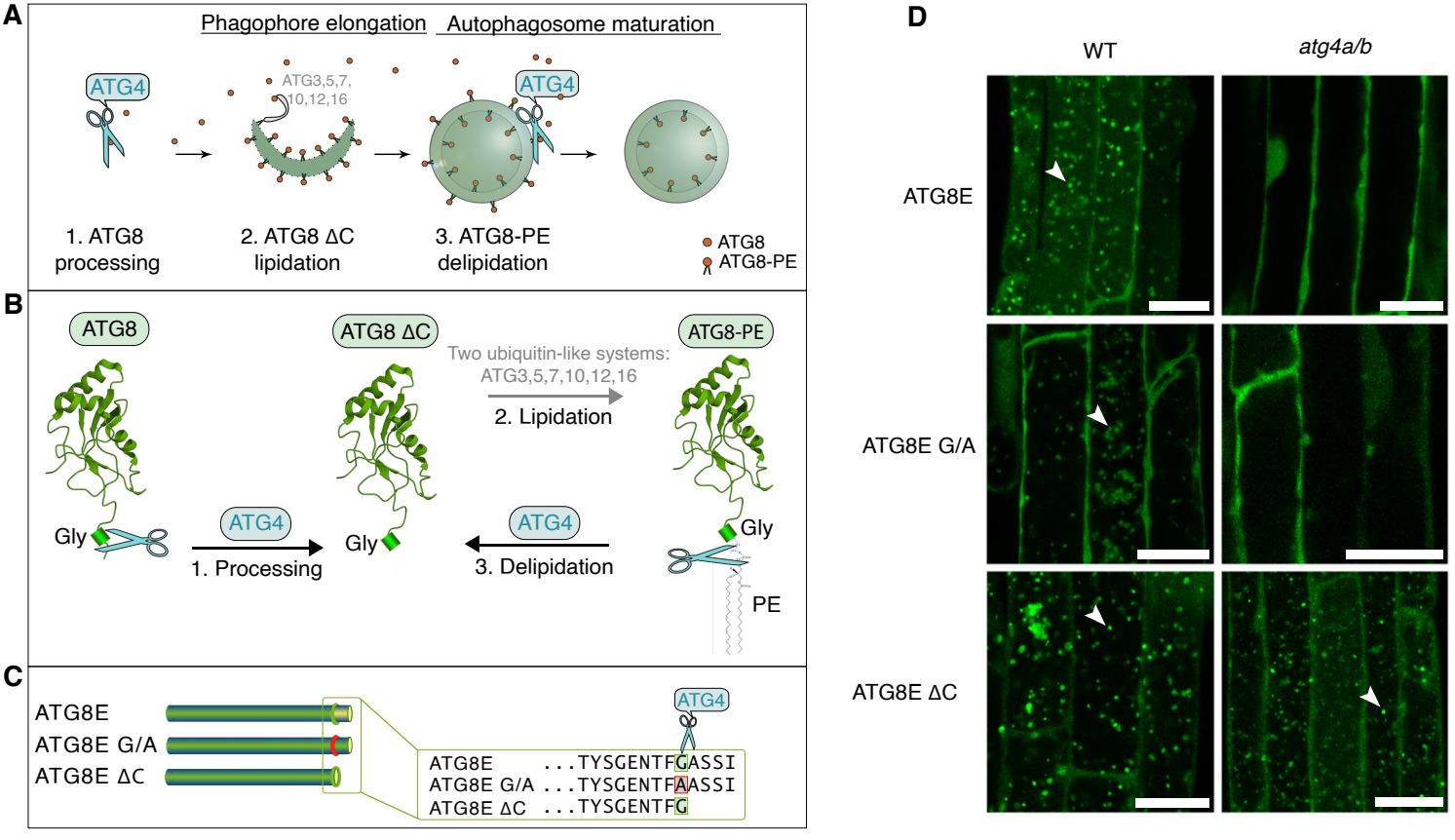


**Figure 1. Post-translational modifications of Arabidopsis ATG8 during autophagy.**

**A**. During autophagosome formation ATG8 must undergo lipidation and delipidation. Lipidation of ATG8 onto phagophore membranes is critical for phagophore elongation. To enable it, ATG8 is first proteolytically processed by ATG4. Lipidated ATG8 is then removed from the outer autophagosomal membrane during maturation of the vesicle.

**B**. ATG8 is constitutively processed by ATG4 to remove the C-terminal peptide. The obtained truncated ATG8 (ATG8 ΔC) has the C-terminal glycine residue exposed for the lipidation reaction. Lipidation of ATG8, i.e., its covalent conjugation to the phosphatidylethanolamine (PE) lipid present in the phagophore membranes (formation of ATG8–PE), is executed by two ubiquitin-like conjugation systems comprising several autophagy-related proteins, including ATG5 and ATG7. Delipidation of ATG8–PE on the outer membrane of autophagosome is performed by the ATG4 protease, which cleaves the amide bond between PE and ATG8, releasing ATG8 ΔC back into the pool of cytoplasmic ATG8 available for autophagosome biogenesis.

**C**. Diagram showing C-terminal sequences of the three artificially created variants of the Arabidopsis isoform ATG8E: ATG8E, full-length protein sequence including the C-terminal peptide masking the critical Gly; ATG8E G/A, full length protein in which the critical Gly residue was replaced with Ala; ATG8E ΔC, truncated protein lacking the C-terminal peptide that was masking the critical Gly.

**D**. Detection of three fluorescently labelled ATG8E variants (shown in **C**) in *Arabidopsis thaliana* epidermal root cells treated with AZD8055 and concanamycin A. WT, wild-type; *atg4a/b*, double knockout of ATG4A and ATG4B genes. Arrowheads indicate autophagic bodies-like puncta inside the vacuoles. Scale bars, 20 µm.

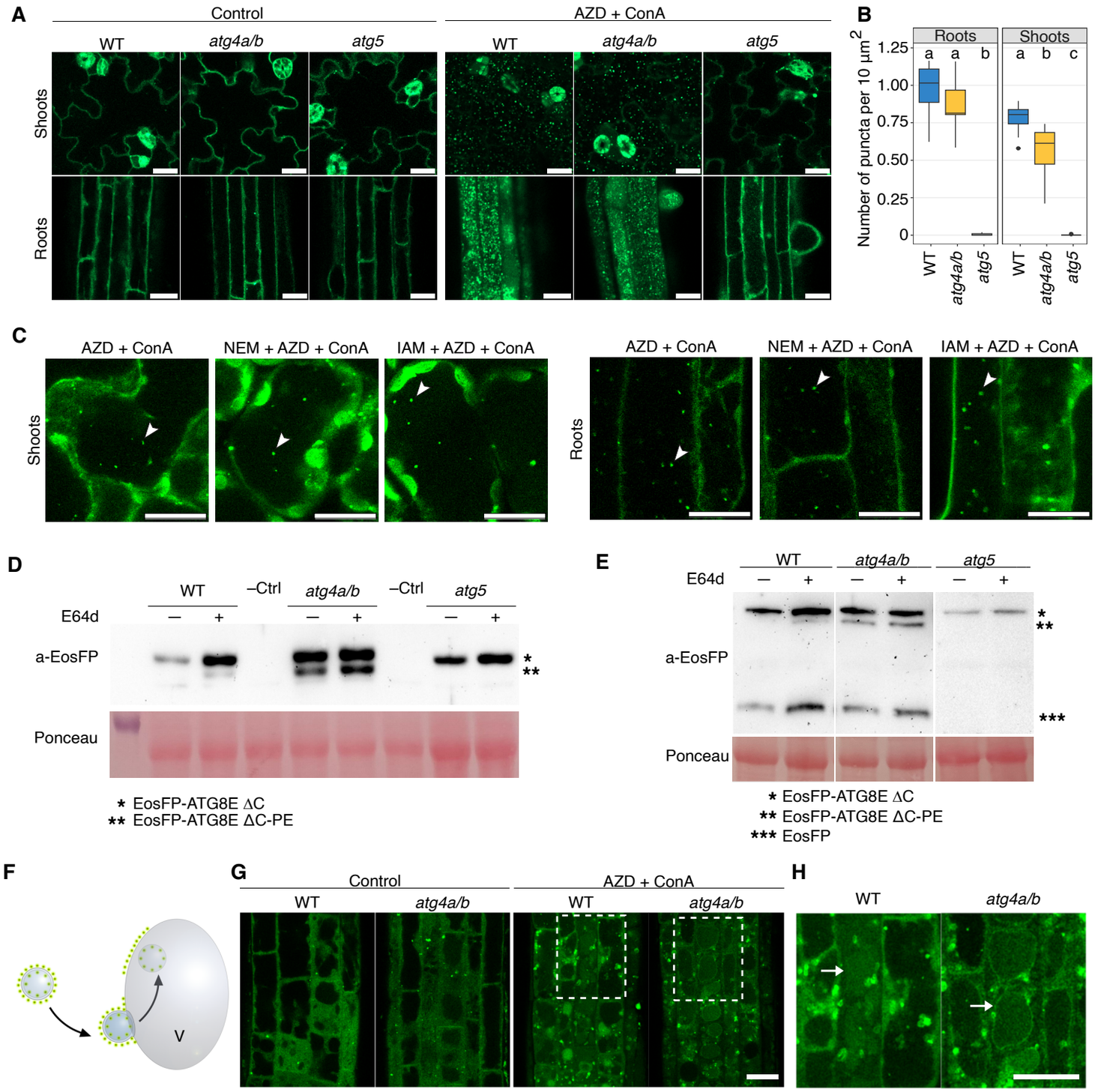


**Figure 2. Delipidation of ATG8E is dispensable for autophagosome formation and their delivery to the vacuoles.**

**A.** Confocal microscopy images of root and shoot epidermal cells of 7-days-old Arabidopsis seedlings expressing EosFP-ATG8E ΔC in WT, ATG4- or ATG5-deficient backgrounds. Seedlings were incubated under control conditions or subjected to AZD/ConA treatment. Scale bars, 20 µm.

**B.** Quantification of puncta per vacuolar area for the samples illustrated in **A**. Tukey's HSD test was performed for each plant organ individually, $n = 40$ for shoots and $n = 29$ for roots. Groups that do not differ are annotated by the same letter ($\alpha = 0.05$). Boxes indicate interquartile region (IQR); median is indicated by a horizontal line; whiskers represent range within 1.5 IQR; outliers are represented by a filled circle. The chart shows representative results of one out of two experiments.

**C.** Confocal microscopy images of EosFP–ATG8E ΔC expressed in mesophyll cell of WT Arabidopsis true leaves (left) or roots of 10 days old seedlings (right) treated with AZD/ConA in the absence or presence of irreversible cysteine protease inhibitors (1mM IAM or 10 mM NEM). Images for leaves were taken at 24 h of treatment, while roots where imaged after 4h of treatment. Time-lapse data confirming that the observed puncta are indeed freely in the vacuoles of leaves is available in the Movie S1.

**D.** Detection of EosFP in the protein extracts of seedlings treated with AZD/ConA and E64d (illustrated in **Fig. S3C and D**). Ponceau S staining was used as a loading control. –Ctrl, negative control (extract of a WT plant with no transgene). Western blot reveals accumulation of the EosFP–ATG8E ΔC–PE in ATG4-deficient background or in WT upon E64d treatment.

**E.** EosFP cleavage assay performed on the same material used for **E** shows no decrease in autophagic activity in the samples accumulating ATG8–PE.

**F.** Schematic representation of EosFP signal accumulation on the tonoplast upon its fusion with EoSP–ATG8E ΔC–decorated autophagosomes in the absence of ATG8-delipidation activity.

**G.** Confocal microscopy images of root epidermal cells expressing EosFP–ATG8E ΔC and showing accumulation of tonoplastic EosFP signal in ATG4-deficeint background upon upregulation of autophagy. Scale bar, 20 µm.

**H.** Zoomed-in images shown in **D** with adjusted contrast. Scale bar, 20 µm.

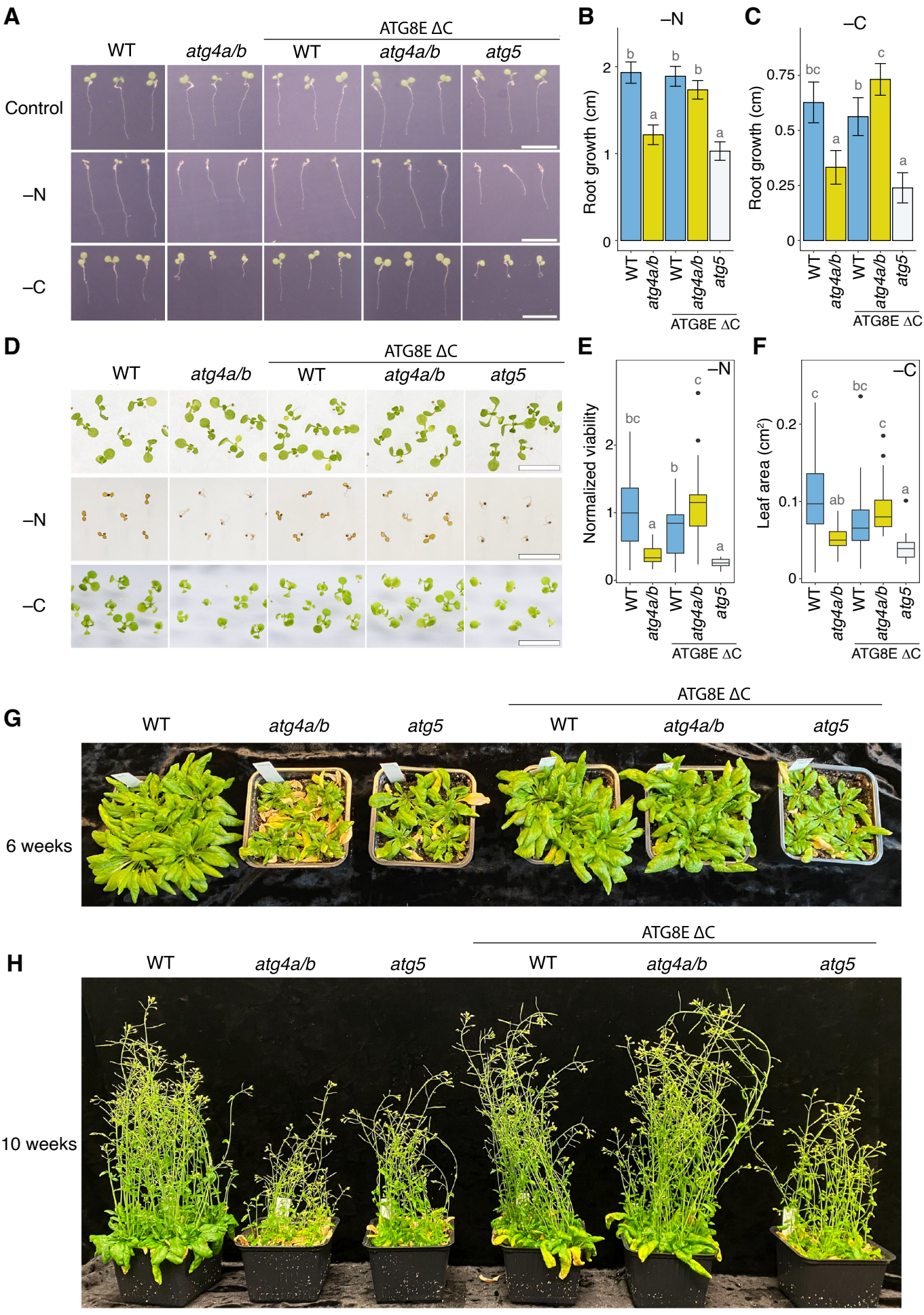


**Figure 3. Expression of ATG8E ΔC alleviates autophagy-deficient phenotypes of *atg4a/b***

**A**. Examples of Arabidopsis seedling roots phenotyped using SPIRO under control, nitrogen-depleted (–N), and carbon-depleted (–C) conditions. Normal root growth under nutrient-depleted conditions is restored in *atg4a/b* seedlings expressing ATG8E ΔC. In total, 997 biological replicates were phenotyped under –N and –C conditions in seven independent experiments.

**B**. Quantification of seedling root length on the 4$^{th}$ day after germination when grown under –N conditions, as illustrated in panel **A** (middle row). Boxes indicate interquartile region (IQR); median is indicated by a horizontal line; whiskers represent range within 1.5 IQR; outliers are represented by solid a filled circle. The chart represents combined data from two independent experiments (n = 364). Root growth was analyzed by fitting a mixed-effect second-order polynomial model to the time-resolved root length data obtained by the SPIRO root growth assay. Letters signify all-pairwise comparisons, where treatments sharing the same letter do not differ at the α = 0.05 level. Error bars indicate 95% confidence interval.

**C**. Quantification of seedling root growth during four days of recovery following four days of carbon depletion, as illustrated in panel **A** (bottom row). Boxes indicate interquartile region (IQR); median is indicated by a horizontal line; whiskers represent range within 1.5 IQR; outliers are represented by solid a filled circle. The chart represents combined data from two independent experiments, *n* = 283. Root length was analyzed and visualized as in **B**.

**D**. Examples of Arabidopsis seedling shoot phenotypes under control, nitrogen-depleted (–N), and carbon-depleted (–C) conditions. Photos of complete plates are shown in **Fig. S4**.

**E**. Viability of Arabidopsis seedlings grown on –N medium illustrated in **D** (middle row) was estimated by shoot chlorosis. Phenotyping was performed in two independent experiments. The chart summarizes data from a single experiment (*n* = 157). The upper and lower edges of boxes indicate upper and lower quartiles of the data, the middle line indicates the median, and the whiskers extend to data points within 1.5 * interquartile range (IQR). Dots indicate data points outside 1.5 * IQR. Tukey's HSD test, shared letters indicate no difference at the α = 0.05 level.

**F**. Efficacy of recovery after carbon-depletion illustrated in **D** (bottom row) was estimated by measuring the leaf area/seedling at the end of a one-week-long recovery after seven days of carbon depletion. The experiment was performed twice. Chart shows representative data from one experiment (*n* = 160). Results were analyzed and visualized as in Panel **E**.

**G**. Rosette phenotype of 6 weeks old plants grown under long day conditions show a typical attribute for autophagy-deficient plants, early onset of senescence, in the *atg4a/b* and *atg5* plants, and lack thereof in the *atg4a/b* plants expressing ATG8E ΔC protein.

**H**. Inflorescence phenotype imaged one month later for the same plants as shown in **G**.

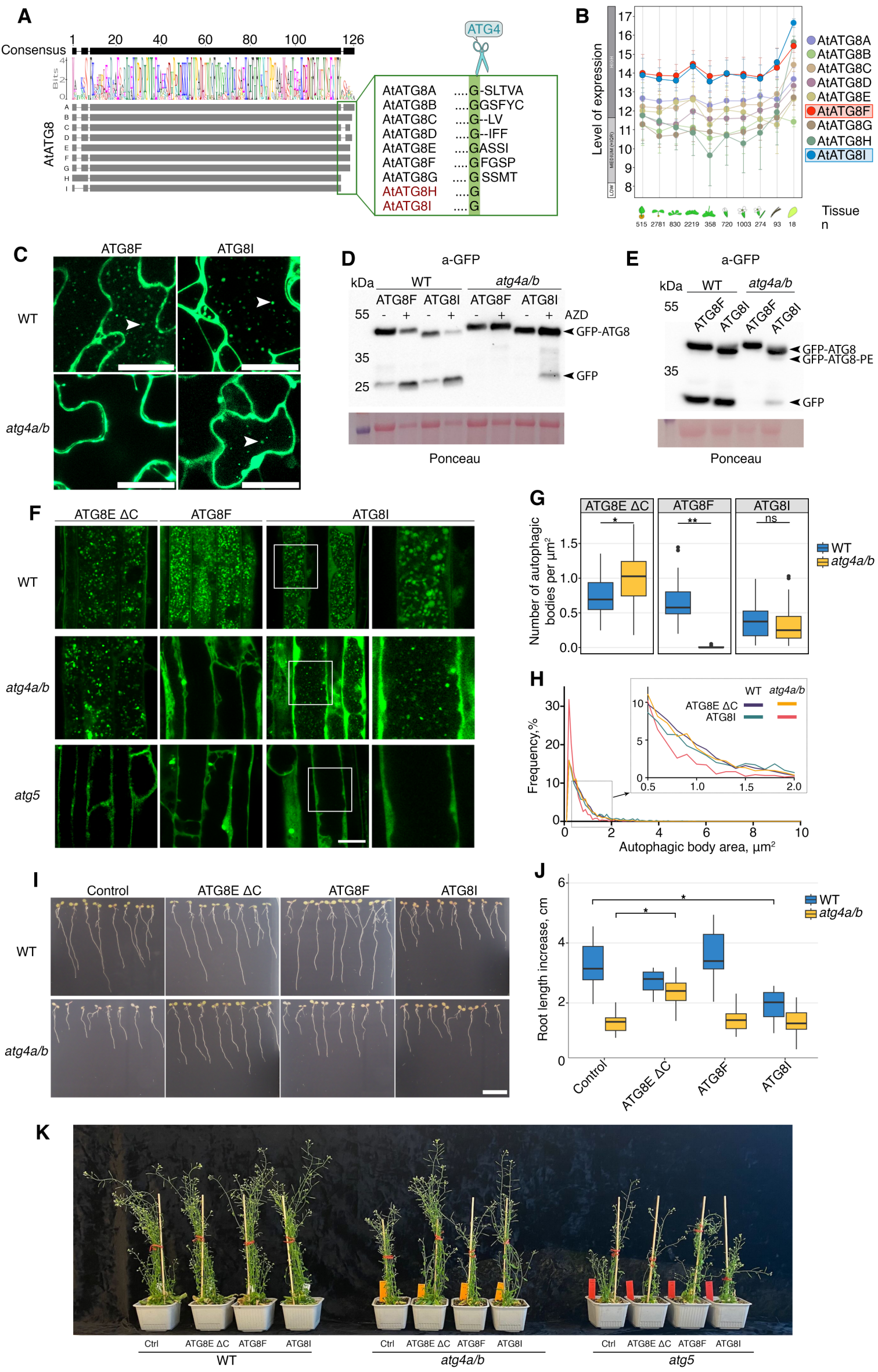


**Figure 4. Arabidopsis ATG8 isoforms differ in their capacity to carry out autophagic flux.**

**A.** Schematic representation of ClustalW protein alignment of the nine Arabidopsis ATG8 isoforms. The inset shows ATG8 C-terminal sequences containing the Gly residue which is critical for lipidation. Notably, ATG8H and ATG8I do not possess the C-terminal peptide and have the critical Gly readily exposed.

**B.** GENEVESTIGATOR data on organ-specific expression of all nine ATG8 isoforms of Arabidopsis. ATG8F (red rectangle) and ATG8I (blue rectangle) isoforms are expressed at the highest level in all tissues.

**C.** Confocal microscopy images showing accumulation of autophagic bodies in the vacuoles of leaf epidermal cells stably expressing GFP-tagged ATG8F or ATG8I in WT or *atg4a/b.* Leaves were infiltrated with AZD/ConA 24 h prior to imaging. White arrowheads point at autophagic bodies. Scale bars, 25 µm.

**D.** GFP cleavage assay performed on the transgenic lines illustrated in **C**, showing restored accumulation of free GFP in the *atg4a/b* plants expressing GFP–ATG8I. Autophagy was induced by infiltrating leaves with AZD 24 h prior to sampling.

**E.** Western blot detection of GFP in AZD-treated samples shown in **D** separated on the gel containing 6 M urea to discern lipidated from non-lipidated forms of ATG8 confirms accumulation of the lipidated ATG8I. The panel shows results representative for two independent experiments.

**F.** Confocal microscopy images showing accumulation of autophagic bodies in root epidermal cells of seedlings expressing three isoforms of Arabidopsis ATG8 (ATG8E ΔC, ATG8F and ATG8I) in the WT, ATG4- or ATG5-deficient backgrounds. Seven days old Arabidopsis seedlings were subjected to AZD/ConA treatment for 24 h prior to imaging. Scale bars, 20 µm.

**G.** Quantification of autophagic bodies in vacuoles of cells illustrated in **F**. Welch's t-test, $n = 337$. *, $p < 0.05$; **, $p < 0.01$; ns, not significant. Boxes indicate interquartile region (IQR); median is indicated by a horizontal line; whiskers represent range within 1.5 IQR; outliers are represented by a filled circle.

**H.** Size distribution of autophagic bodies in the samples illustrated in **F** and quantified in **G**. The inset shows a magnified portion of the chart visualizing the higher frequency of smaller autophagic bodies present in the vacuoles of *atg4a/b* plants expressing ATG8I.

**I.** Root growth phenotype of 12-days-old seedlings incubated for 7 days on nitrogen depleted medium. Expression of native truncated ATG8I isoform is not sufficient to alleviate the autophagy-deficient phenotype of *atg4a/b*. Seedlings were grown for 4 days on standard 0.5xMS medium, checked for GFP signal, then transferred onto –N medium plates to be imaged for 7 days.

**J.** Quantification of the increase in root length of the seedlings after 7 days growth on the –N medium (illustrated in **I**). The experiment was performed three times. Boxes indicate interquartile region (IQR); median is indicated by a horizontal line; whiskers represent range within 1.5 IQR; outliers are represented by solid a filled circle. The chart shows representative data from one experiment. Dunnett's tests were performed for WT and *atg4a/b* separately, comparing each genotype against the control sample ($n$ =128). *, $p < 0.0001$.

**K**. Phenotypes of two months old plants grown in soil under long day conditions. Photos show plants with representative phenotypes, the experiment was performed twice using four biological replicates for each genotype. Ctrl, a not transformed plant of the corresponding genotype; ATG8E ΔC, ATG8F and ATG8I, overexpression of the fluorescent fusion of the corresponding ATG8 isoform.

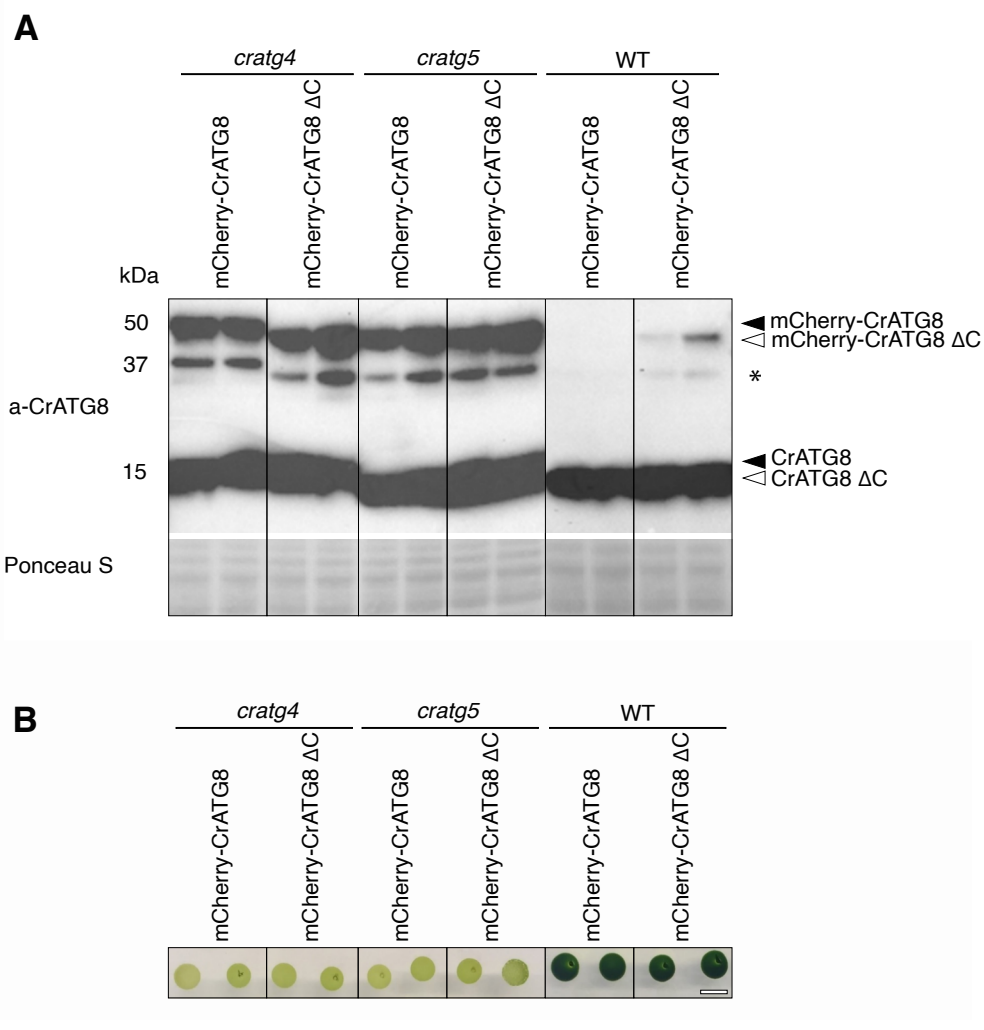


**Figure 5. Delipidation of ATG8 is critical for autophagy in *Chlamydomonas reinhardtii*.**

**A.** Western blot detection of endogenous ATG8 and mCherry–CrATG8 transgene expression in the WT, *cratg4,* and *cratg5* backgrounds. Ponceau S staining was used as a loading control. The cells were grown in the liquid TAP medium under standard conditions and harvested at a density of 1-2×107 cells $ml^{-1}$. *, a putative product of autophagy-independent proteolytic processing of mCherry-CrATG8.

**B.** Senescence phenotype of the transgenic *Chlamydomonas* lines grown on the TAP medium for 40 days. Light color of colonies indicates nutrient deficiency sensitivity caused by dysfunctional autophagy. Scale bar, 1 cm.

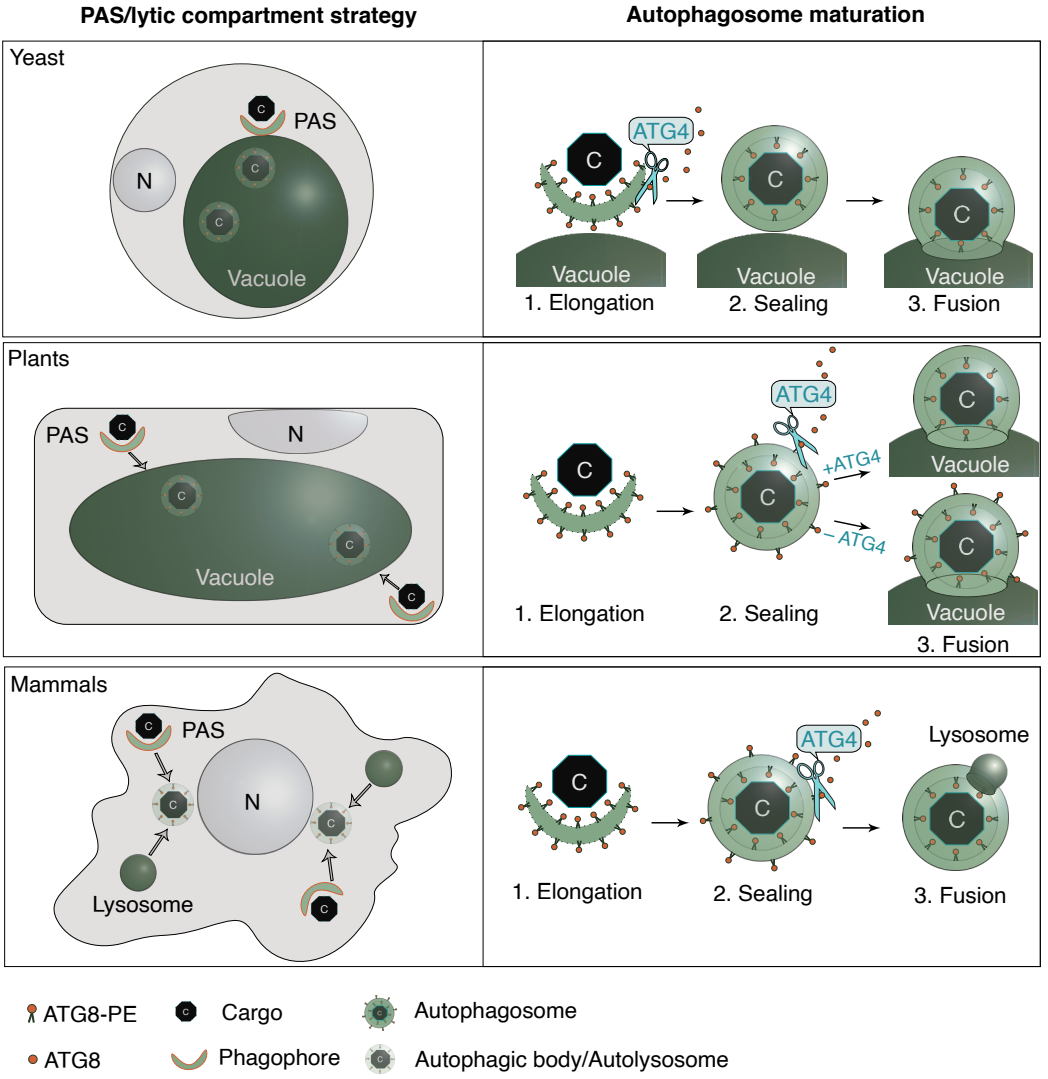


**Figure 6. Schematic representation of ATG8 delipidation importance for autophagy in the three eukaryotic kingdoms.**

ATG4-dependent delipidation of ATG8 is considered to be generally conserved in plants, animals and fungi. However, this process is critical for early steps of autophagosome maturation in yeast cells (phagophore elongation), while in mammalian cells the same delipidation step is critical for the later stage of autophagy (docking of complete autophagosomes to lysosomes). In this study we show that although ATG8 delipidation occurs in plants, it is dispensable for autophagy.

The different roles ATG8-delipidation plays in autophagosome maturation might be representative of autophagy adaptation to the various strategies for the lytic compartment (single large immobile vacuoles in plant and yeast cells *vs* numerous small motile lysosomes in animal cells), for phagophore assembly sites (single site in yeast *vs* numerous sites in animal and plant cells), and autophagosome trafficking towards the lytic compartment (autophagosome formation in the proximity to the vacuole in yeast, trafficking of autophagosomes towards immobile vacuole in plants, coordinated trafficking of autophagosomes and lysosomes to their meeting spot in mammalian cells).

C, cargo; N, nucleus.

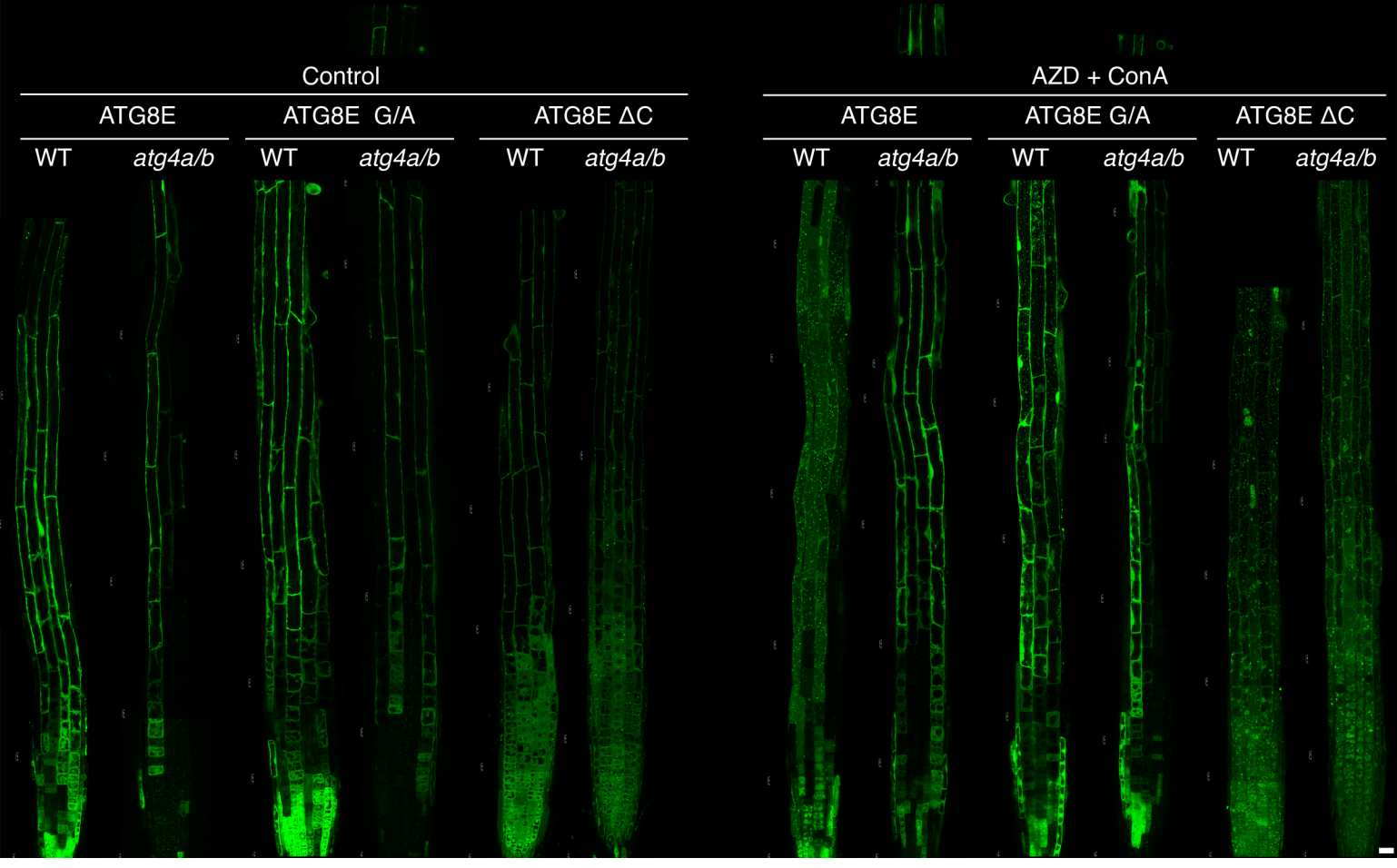


**Figure S1**. **Expression of ATG8E ΔC restores accumulation of puncta in the vacuoles of ATG4-deficeint Arabidopsis roots.**

Complete tile-scans of roots partially shown in **Fig. 1 D**. Control, roots incubated and imaged in the standard 0.5xMS growth medium; AZD + ConA, roots incubated and imaged in the 0.5xMS medium supplemented with 5 µM AZD8055 and 0.5 µM concanamycin A. Scale bar, 20 µm.

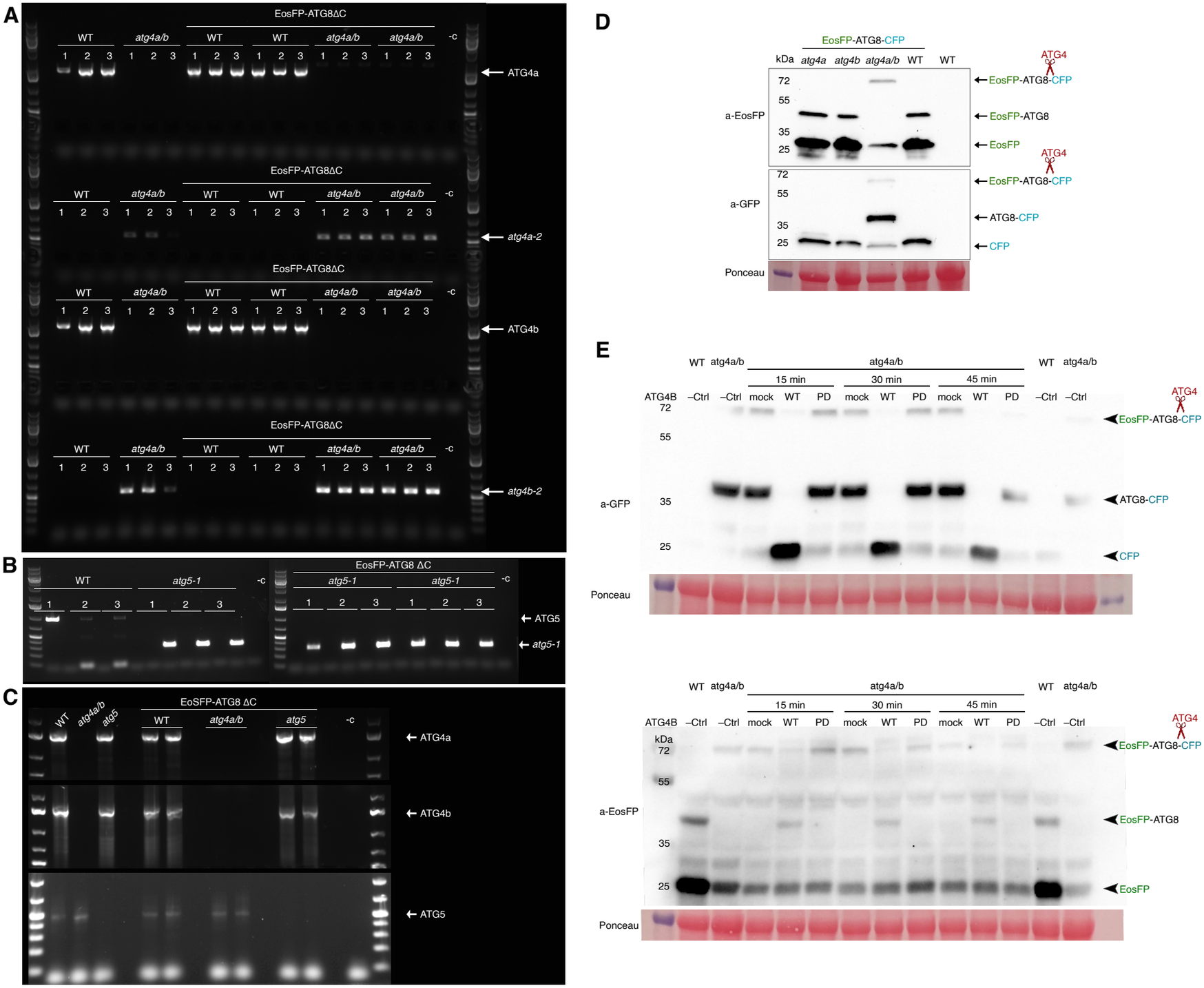


**Figure S2. Verification of the transgenic lines used in the study.**

**A**. Genotyping of Arabidopsis lines to detect WT *ATG4A* and *ATG4B* alleles as well as *atg4a-2* and *atg4b-2* T-DNA insertions. The results confirm absence of complete *ATG4* genes in all lines with *atg4a/b* background.

**B**. Genotyping of Arabidopsis lines to detect WT *ATG5* allele as well as *atg5-1* T-DNA insertion.

**C**. RT-PCR confirms absence of full length *ATG4* mRNAs in the *atg4a/b* lines. Similarly, *atg5-1* lines do not contain full length *ATG5* transcript.

**D**. Lack of ATG4 proteolytic activity in the *atg4a/b* double knockout was confirmed by Western blot detection of the EosFP–ATG8–CFP fusion protein in the total protein extracts of plants stably expressing the fusion in the WT, *atg4a*, *atg4b,* and *atg4a/b* backgrounds. The product of cleavage by ATG4, EosFP–ATG8, was not detectable in the *atg4a/b* knockout line. Notably expression of either of the ATG4 proteases is sufficient to process all the ectopically overexpressed EosFP–ATG8–CFP fusion protein.

**E**. Processing of the EosFP–ATG8–CFP fusion by ATG4 protease was corroborated in the *in vitro* assay. Total protein extracts of plants stably expressing EosFP–ATG8-CFP fusion in *atg4a/b* background was incubated together with a buffer (mock), recombinant active ATG4B (WT) or its proteolytically dead mutant (PD) for 15, 30, or 45 min. The reactions were loaded on the polyacrylamide gel and subjected to Western blotting detecting EosFP tag. Additionally, total protein extracts of plants expressing the same fusion protein in the WT and ATG4-deficient background were mixed directly with loading buffer and used as additional controls for fusion protein stability *in vivo* (WT –Ctrl and *atg4a/b* –Ctrl, respectively). Cleavage of the bond between ATG8 and CFP was observed only in the presence of active ATG4.

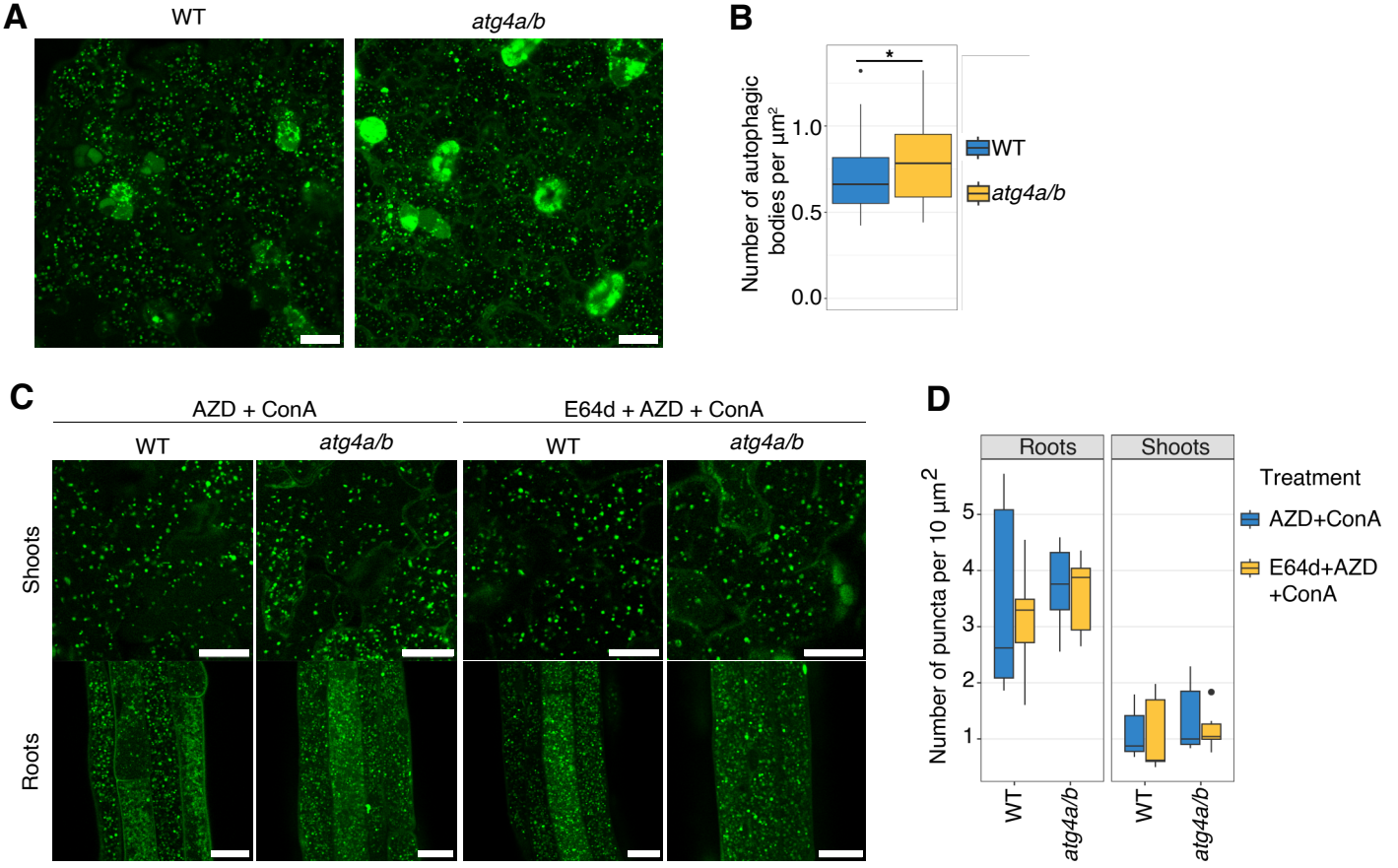


**Figure S3. Detection of autophagic bodies in true leaves of plants expressing ATG8E ΔC.**

**A**. Confocal microscopy images of leaf epidermal cells of 1.5-months-old Arabidopsis plants expressing EosFP–ATG8E ΔC in WT or ATG4-deficient backgrounds. Leaves were infiltrated with AZD/ConA solution 24 h prior to imaging. Scale bars, 20 µm.

**B.** Quantification of puncta per vacuolar area for the samples illustrated in **A**. The chart shows representative results of one out of two experiments, $n = 90$. The samples differ according to Welch's *t*-test, *, $p < 0.05$. Boxes indicate interquartile region (IQR); median is indicated by a horizontal line; whiskers represent range within 1.5 IQR; outliers are represented by solid a filled circle.

**C.** Confocal microscopy images of root and shoot epidermal cells of 7-days-old Arabidopsis seedlings expressing EosFP–ATG8E ΔC in WT or *ATG4* knockout. Seedlings were treated for 8 h with the cysteine protease inhibitor E64d prior to induction of autophagy with AZD/ConA. Scale bars, 20 µm.

**D.** Quantification of puncta per vacuolar area on the data illustrated in **C**. Tukey's HSD test was performed for each plant organ individually, no statistically significant difference was discovered at the $\alpha = 0.05$ level; $n = 36$ for each organ. Boxes indicate interquartile region (IQR); median is indicated by a horizontal line; whiskers represent range within 1.5 IQR; outliers are represented by a filled circle. The chart shows representative results for one out of two experiments.

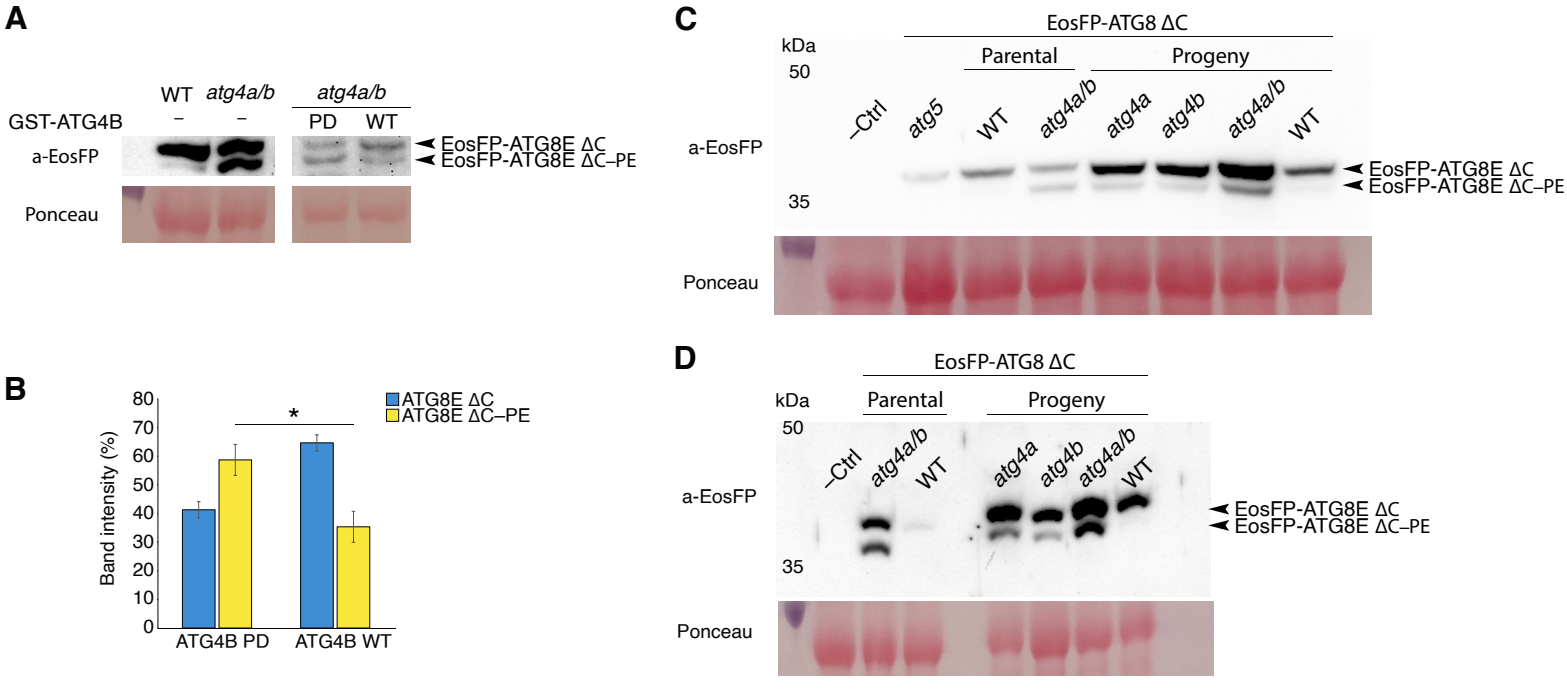


**Figure S4. Efficient delipidation of ATG8E ΔC in Arabidopsis requires expression of both ATG4 proteases.**

**A**. *In vitro* ATG8 delipidation assay. Left panels: higher accumulation of the ATG8–PE adduct in *atg4a/b* plants expressing EosFP-ATG8E ΔC compared to WT was confirmed by immunodetection of EosFP in total protein extracts obtained by mixing plant material with hot Laemmli buffer. Right panels: total protein extract of *atg4a/b* plant expressing EosFP-ATG8E ΔC was incubated with recombinant active GST-ATG4B (WT) or its proteolytically dead mutant (PD) prior to Western blot detection of the EosFP tag. Ponceau S staining was used as a loading control.

**B**. Quantification of the EosFP–ATG8E ΔC and EosFP– ATG8E ΔC–PE bands intensity illustrated in **A** shows significant decrease in the ATG8–PE content in the presence of active ATG4B. Band intensity is expressed as a percentage of the sum intensity for both bands in each sample. Error bars indicate StDev. Chart shows results for two independent experiments. Student's t-test at the $\alpha = 0.05$ level; *, $p < 0.001$, $n = 24$.

**C**. Western blot detection of EosFP tag in the total protein extract of 14-days-old Arabidopsis seedlings expressing EosFP–ATG8E ΔC in the WT, ATG5-, ATG4A-, ATG4B-, and ATG4A/B-deficient backgrounds. Sampling was done without any prior treatment. –Ctrl, negative control (extract of Arabidopsis seedlings not expressing EosFP tagged proteins). Ponceau S staining was used as a loading control. Single *ATG4*-knockout plants were obtained by crossing *atg4a/b* plants with WT. Parental, plants grown from seed used for crossing; progeny, plants grown from F2 generation seeds obtained from the crosses. Seedlings were genotyped prior to protein extraction to confirm the genetic background.

**D**. Detection of the EosFP–ATG8–PE form in the total protein extracts from 1.5-months-old plants corroborates observations made on seedlings and illustrated in **A**: both ATG4 proteases are required for efficient delipidation of ATG8E ΔC. Sampling was done without any prior treatment.

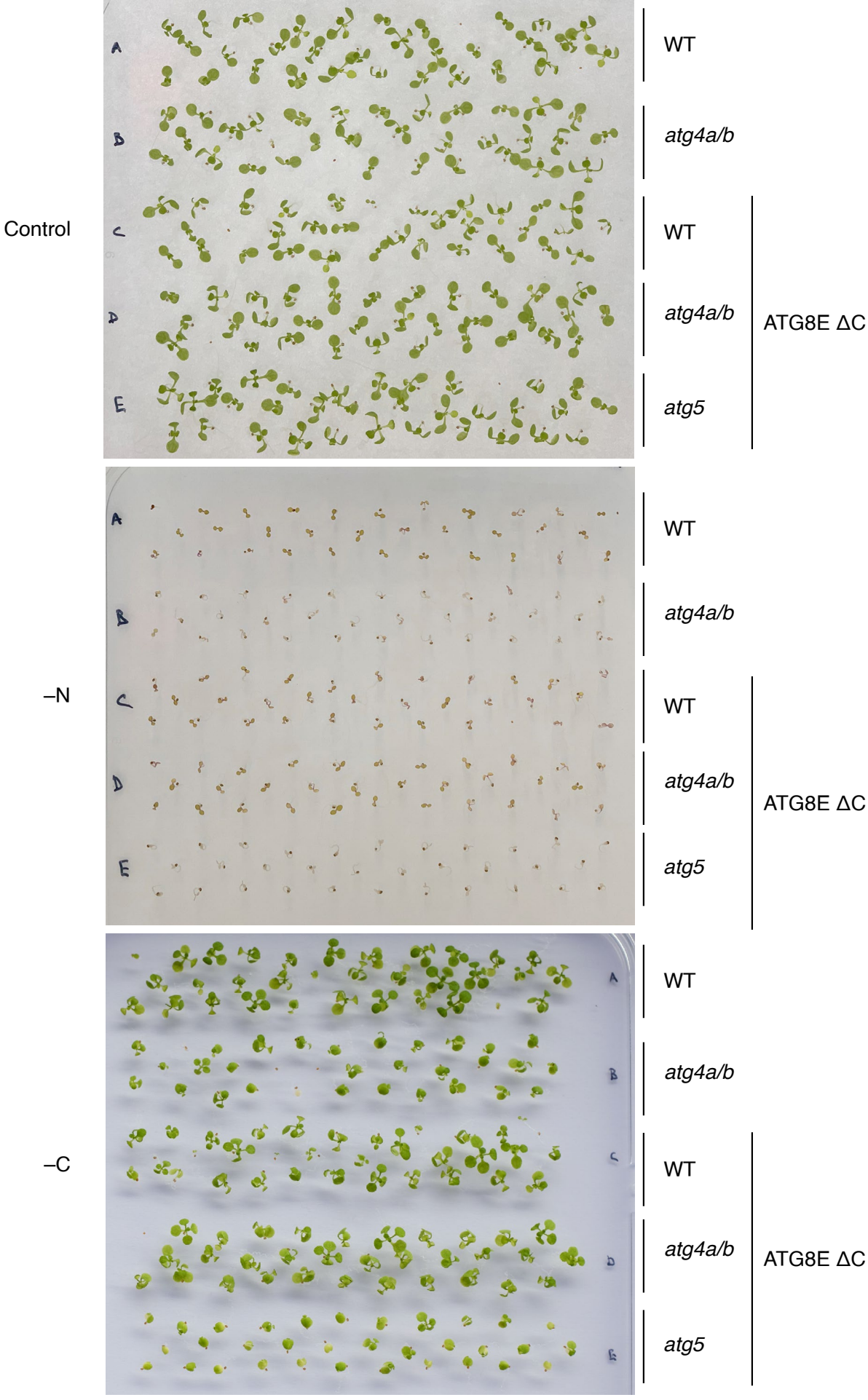


**Figure S5. Expression of ATG8E ΔC complements autophagy-deficient shoot phenotypes of *atg4a/b*.**

Images of Petri plates with Arabidopsis seedlings grown on 0.5x MS medium (Control), nitrogen-depleted (–N) medium or carbon-depleted (–C) medium. Autophagy-deficient seedlings have decreased viability under –N conditions (quantification shown **Fig. 3E**). However, *atg4a/b* seedling expressing ATG8E ΔC exhibit wild-type-like viability. Seedlings grown on –C medium were subjected to seven days of dark treatment followed by seven days of recovery prior to imaging. Autophagy-deficient seedlings are slower to recover compared to both wild-type seedlings and *atg4a/b* seedlings expressing ATG8E ΔC (quantification shown **Fig. 3F**).

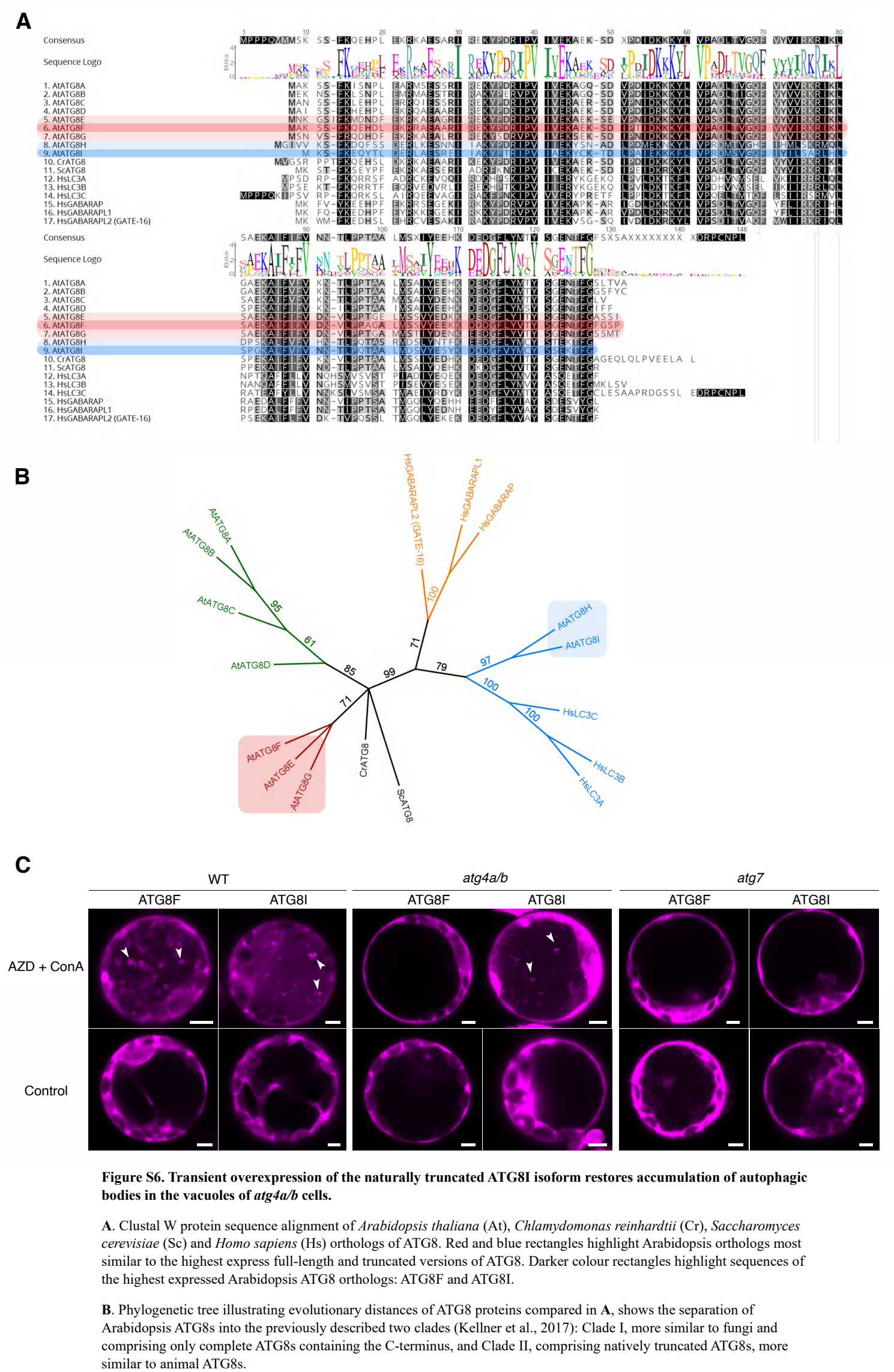


**Figure S6. Transient overexpression of the naturally truncated ATG8I isoform restores accumulation of autophagic bodies in the vacuoles of *atg4a/b* cells.**

**A**. Clustal W protein sequence alignment of *Arabidopsis thaliana* (At), *Chlamydomonas reinhardtii* (Cr), *Saccharomyces cerevisiae* (Sc) and *Homo sapiens* (Hs) orthologs of ATG8. Red and blue rectangles highlight Arabidopsis orthologs most similar to the highest express full-length and truncated versions of ATG8. Darker colour rectangles highlight sequences of the highest expressed Arabidopsis ATG8 orthologs: ATG8F and ATG8I.

**B**. Phylogenetic tree illustrating evolutionary distances of ATG8 proteins compared in **A**, shows the separation of Arabidopsis ATG8s into the previously described two clades (Kellner et al., 2017): Clade I, more similar to fungi and comprising only complete ATG8s containing the C-terminus, and Clade II, comprising natively truncated ATG8s, more similar to animal ATG8s.

**C**. mScarlet–ATG8F or mScarlet–ATG8I were transiently expressed in mesophyll protoplasts of WT, *atg4a/b,* or *atg7* Arabidopsis plants. An aliquot of each transformed protoplast suspension was subjected to AZD/ConA treatment for 17 h prior to imaging. Scale bar = 5 µm. White arrow heads indicate autophagic bodies.

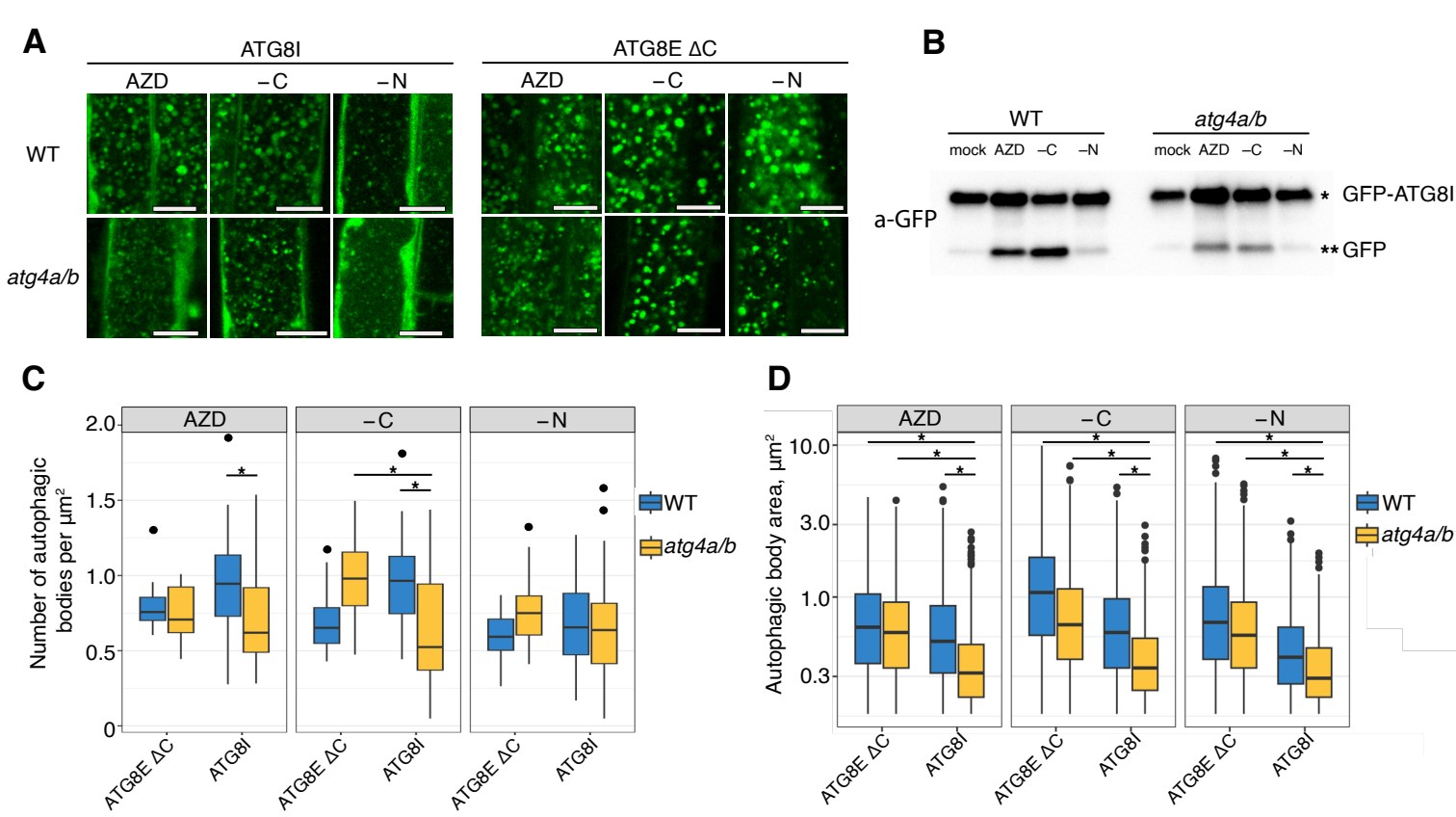


**Figure S7. Overexpression of the naturally truncated ATG8I isoform in the WT leads to a decreased autophagic activity efficiency under nitrogen-depleted conditions.**

**A.** Confocal microscopy images showing phenotypes of autophagic bodies in the vacuoles of root epidermal cells of seedlings expressing ATG8E ΔC or ATG8I in WT and *atg4a/b* backgrounds. Seven days old Arabidopsis seedlings were subjected to treatments for 24 h prior to imaging. The treatments included AZD/ConA, –C/ConA , and –N/ConA. Scale bars, 10 µm.

**B.** GFP cleavage assay performed on the seedlings illustrated in **A** confirms autophagic activity under all three stress conditions used in the experiment.

**C**. Quantification of autophagic bodies for the data illustrated in **A** confirms autophagic activity under all three conditions used in the experiment. Boxes indicate interquartile region (IQR); median is indicated by a horizontal line; whiskers represent range within 1.5 IQR; outliers are represented by solid a filled circle. Dunnett's test vs *atg4a/b* expressing ATG8I was performed for each treatment. *, $p < 0.0001$. Dots indicate outliers.

**D**. Quantification of puncta areas in the samples illustrated in **A** reveals significant decrease of autophagic body size under nitrogen depleted conditions if ATG8I is overexpressed either in the WT or *atg4a/b* backgrounds. Boxes indicate interquartile region (IQR); median is indicated by a horizontal line; whiskers represent range within 1.5 IQR; outliers are represented by solid a filled circle. Dunnett's test vs *atg4a/b* expressing ATG8I was performed for each treatment. *, $p < 0.0001$. Dots indicate outliers.

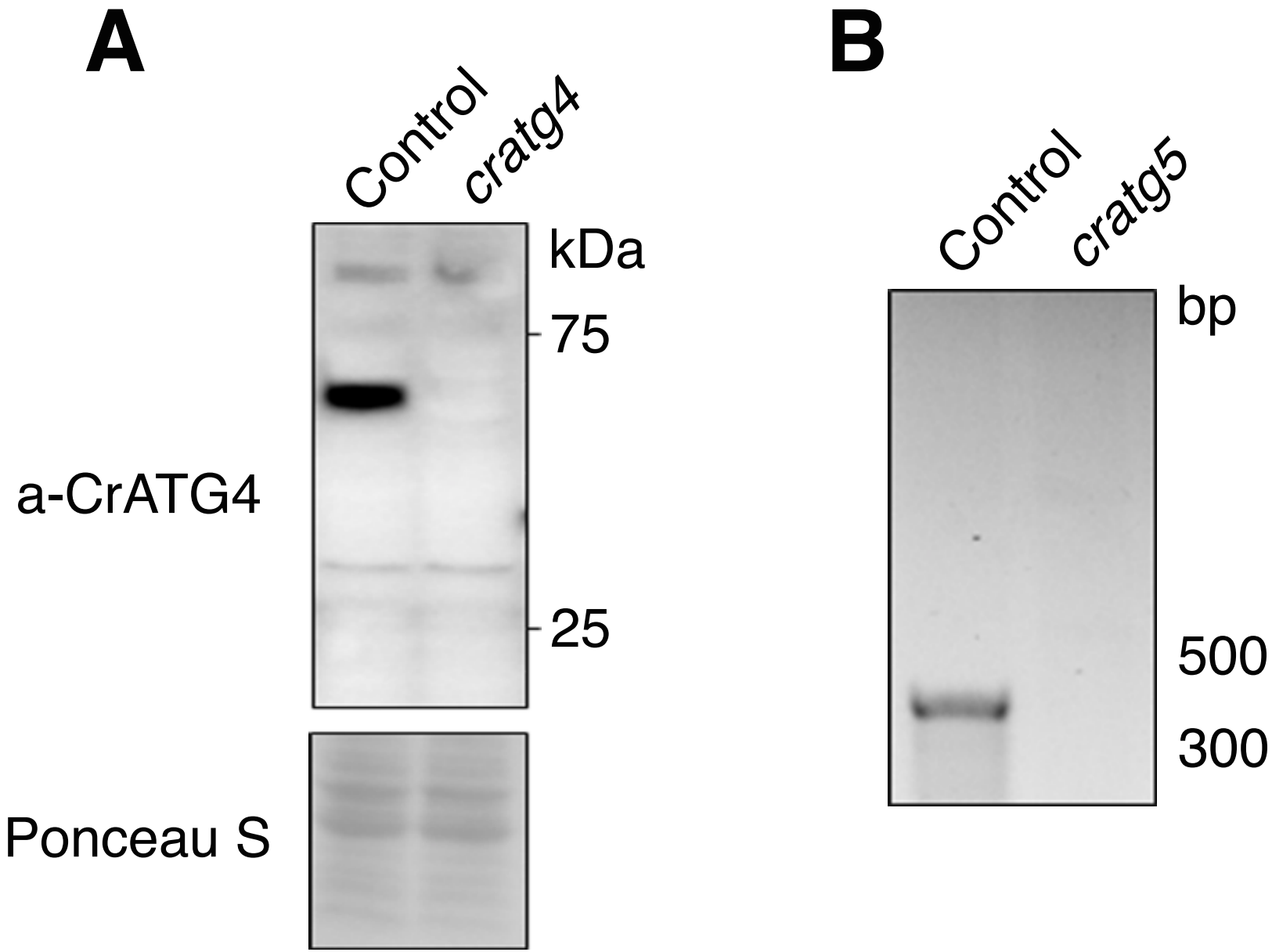


**Figure S8. Validation of generated *Chlamydomonas ATG4* and *ATG5* knockout mutants.**

**A**. Western blot detection of ATG4 protein in the total protein extracts of WT (Control) and *ATG4* knockout (*cratg4*) *Chlamydomonas* cells confirms absence of ATG4 protein in the knockout background. Ponceau S staining was used as a loading control.

**B**. Genotyping of the *ATG5* knockout mutant confirms deletion of the *ATG5* gene.